A 12 GeV Research Proposal to Jefferson Lab (PAC 38)

Studies of Dihadron Electroproduction in DIS with Unpolarized and Longitudinally Polarized Hydrogen and Deuterium Targets

H. Avakian[†*], V.D. Burkert, L. Elouadrhiri, V. Kubarovsky
Jefferson Lab, Newport News, VA 23606, USA

S. Anefalos Pereira[†], M. Aghasyan, E. De Sanctis,D. Hasch, L. Hovsepyan,
V. Lucherini, M. Mirazita, S. Pisano, and P. Rossi
INFN, Laboratori Nazionali di Frascati , Frascati, Italy

A. Courtoy[†], A. Bacchetta, M. Radici
Universita' di Pavia and INFN Sezione di Pavia, via Bassi 6, 27100 Pavia, Italy

L. Pappalardo[†], L. Barion, G. Ciullo, M. Contalbrigo, P.F. Dalpiaz,P. Lenisa, M. Statera
University of Ferrara and INFN Ferrara, Via Saragat, I-44100, Ferrara, Italy

K. Griffioen[†], Bo Zhao
College of William & Mary, VA 23187, USA

K. Joo, P. Schweitzer, M. Ungaro
University of Connecticut, Storrs, CT 06269, USA

G. De cataldo, R. De Leo, L. La Gamba, E. Nappi
University of Bari and INFN Bari, Via Orabona, I-70125, Bari, Italy

M. Battaglieri, A. Celentano, R. De Vita, M. Osipenko, G. Ricco, M. Ripani, M. Taiuti
Dipartamento di Fisica and INFN, Sezione di Genova, Via Dodecaneso, 33 I-16146 Genova, Italy

V. Bellini, A. Giusa, F. Mammoliti, R. Potenza, G. Russo, L. Sperduto, C. Sutera
University of Catania and INFN Catania, Via S. Sofia, I-95123 Catania, Italy

R. Perrino
INFN Lecce, Via Arnesano, I-73100 Lecce, Italy

A. D'Angelo, C. Schaerf, I. Zonta
Dipartimento di Fisica, Universita' di Roma Tor Vergata,
INFN Sezione di Roma Tor Vergata, Via della Ricerca Scientifica, I-00133, Rome, Italy

F. Meddi, G.M. Urciuoli
INFN Roma I, P.le aldo Moro, I-00185, Roma, Italy

E. Cisbani, A. Del Dotto, F. Garibaldi, S. Frullani
INFN Roma I and Istituto Superiore di Sanita', Viale Regina Elena, I-00161, Roma, Italy

M. Capogni
INFN Roma I and ENEA Casaccia, Via Anguillarese, I-00123, Roma, Italy

B. Briscoe, I. Strakovsky
The George Washington University, Washington, DC 20052, USA

M. Anselmino, A. Kotzinian, B. Parsamyan

Università di Torino and INFN, Sezione di Torino, Via P. Giuria 1, I-10125 Torino

L. Trentadue
Universita' di Parma, Dipartimento di Fisica e INFN Gruppo Collegato di Parma,
Sezione di Milano Bicocca, Via G.P. Usberti, 7/a 43100 Parma

A. Mukherjee
Department of Physics, Indian Institute of Technology Bombay Powai,
Mumbai 400076, India

M. Wakamatsu
Department of Physics, Faculty of Science, Osaka University,
Toyonaka, Osaka 560-0043, Japan

A CLAS collaboration proposal

† Co-spokesperson * Contact: Harut Avakian, JLab,Newport News VA 23606. Email: avakian@jlab.org

Collaborators' commitment to the 12 GeV upgrade of Jefferson Lab

- ### Italian JLAB12 collaboration

  The Italian JLAB12 collaboration (INFN Bari, INFN Catania, Laboratori Nazionali di Frascati, INFN Genova, INFN Roma I and Istituto Superiore di Sanita', INFN Roma Tor Vergata) is actively involved in this proposal. Among CLAS12 equipment, the group plans to contribute to the design, prototyping, construction and testing of the CLAS12 RICH detector and central calorimeter. Seven staff members and three post-docs will spend their time as needed on this project. Funding for the group is from the Italian research agency Istituto Nazionale di Fisica Nucleare (INFN). Additional funding are planned to be sought in the European Community.

- ### The College of William and Mary

  The College of William and Mary group is actively involved in this proposal, as well as several other proposals using CLAS12. Other members of our group are also pursuing proposals and construction projects in Hall A. The group is playing a role in the design and construction of the pre-shower calorimeter for CLAS12. Together with JMU, NSU, OU, JMU and JLab, the group has an NSF MRI grant that funds procurement of much of the detector components and initial labor for component construction. The group is responsible for scintillator work including R&D for the scintillator/wave-length-shifting fiber specifications and configuration, procurement of fibers, precision cutting of the scintillator bars into the triangular shapes for 15 planes in 5 sectors, and quality control of scintillators and fibers. The group will also provide technical manpower for assembly of the calorimeters. This effort has involved two faculty members, a research engineer, a post-doc, a graduate student, and several undergraduates. Funding for the group is from the DOE and the NSF. One member serves on the CLAS12 Coordinating Committee. Facilities at William and Mary used for this include a 2000 square foot high bay and smaller research labs, including a clean room.

Abstract

We are proposing a comprehensive program to study quark gluon correlations in semi-inclusive electroproduction of hadron pairs using the upgraded JLab 11 GeV polarized electron beam and the CLAS12 detector with unpolarized and longitudinally polarized proton and deuteron targets. The large acceptance of CLAS12 will allow simultaneous detection of the scattered electrons and hadrons from the hadronization of the struck quarks and target fragments, providing information on flavor and transverse momentum of underlying distribution functions. Pairs of hadrons detected in the current fragmentation region allow us to study higher twist distribution functions describing quark-gluon correlations and chiral-odd Dihadron Fragmentation Functions (DiFF) describing correlations between the transverse polarization of the fragmenting quark and the azimuthal orientation of the plane containing the detected hadron pair.

The study of two-hadron production – both in the current fragmentation region (CFR) and also in the target fragmentation region (TFR) – in polarized SIDIS provides information on the nucleon structure and hadronization dynamics that complements single-hadron SIDIS. The leading-order azimuthal asymmetries in particular provide access to polarized TMD Fracture Functions, which are the conditional probabilities of producing a hadron h in the TFR when hard scattering occurs on quark q from the target nucleon N.

Kinematical dependences of the $\sin\phi$ moments for the CFR and TFR regions will be studied to probe the underlying distribution and fragmentation functions. Studies with kaons, enabled by the CLAS12 RICH detector, together with pions, will provide crucial flavor-dependence of the corresponding structure functions.

The experiment will use the upgraded CLAS12 detector, an 11 GeV highly polarized electron beam, and unpolarized hydrogen and deuterium as well as longitudinally polarized solid ammonia targets (NH_3 and ND_3). We request 56 days of running on unpolarized hydrogen and deuterium, 30 days of running on NH_3 and 50 days of running on ND_3 (or possibly ^{6}Li D or HD), plus about 20% overhead for target anneals, polarization reversal, and auxiliary measurements. This experiment will run simultaneously with already approved measurements using pion electroproduction.

Contents

1 Introduction

In recent years, measurements of azimuthal moments of polarized hadronic cross sections in hard processes have emerged as a powerful tool to probe nucleon structure. Many experiments worldwide are currently trying to pin down various effects related to the nucleon structure through semi-inclusive deep-inelastic scattering (HERMES at DESY [1, 2, 3, 4], COMPASS at CERN [5], at Jefferson Lab [6, 7, 8, 9]) polarized proton-proton collisions (PHENIX, STAR and BRAHMS at RHIC) [10, 11, 12], and electron-positron annihilation (Belle at KEK) [13, 14]. Azimuthal distributions of final state particles in semi-inclusive deep inelastic scattering, in particular, are sensitive to the orbital motion of quarks and play an important role in the study of transverse momentum distributions (TMDs) of quarks in the nucleon.

Significant azimuthal moments in leptoproduction ($A_{UU}^{\cos\phi}$) which have been measured in SIDIS already by EMC collaboration [15, 16], were reproduced by latest measurements at CERN, HERMES and JLab [8, 9, 17, 18, 19, 20]. The first unambiguously measured single spin phenomena in SIDIS, which triggered important theoretical developments, were the sizable longitudinal target ($A_{UL}^{\sin\phi}$) and beam ($A_{LU}^{\sin\phi}$) spin asymmetries observed at HERMES and JLab [1, 2, 21, 6, 22, 7, 4], could be interpreted in terms of higher twist distribution functions. In this proposal, we intend to measure similar asymmetries in semi-inclusive production of two hadrons, which offer a cleaner access to collinear twist-3 distributions.

At Twist-3, and before integration over transverse momentum, there are 16 distribution functions (see Tab. 1) for different combinations of target (rows in Tab. 1) and quark (columns in Tab. 1) polarizations. Only three functions survive integration over transverse momentum (collinear functions): e, h_L and g_T. Together with the twist-2 PDFs (f_1, g_1, h_1), they give a detailed picture of the nucleon in longitudinal momentum space. The main goal of the present proposal is to access the functions e and h_L. Higher twist (HT) functions are of interest for several reasons. Most importantly they offer insights into the physics of the largely unexplored quark-gluon correlations which provide direct and unique insights into the dynamics inside hadrons, see, e.g., [23]. They describe multiparton distributions corresponding to the interference of higher Fock components in the hadron wave functions, and as such have no probabilistic partonic interpretations. Yet they offer fascinating doorways to studying the structure of the nucleon. The third Mellin moment of the HT function e, for instance, describes the average transverse force acting on a transversely polarized quark in an unpolarized target after interaction with the virtual photon [24].

HT contributions are also indispensable to correctly extract twist-2 parts from data. Although suppressed with respect to twist-2 observables by $1/Q$, twist-3 observables are not small in the kinematics of fixed target experiments. This is illustrated by the fact that the twist-3 asymmetry $A_{UL}^{\sin\phi}$ is a large and cleanly seen effect, while the twist-2 asymmetry $A_{UL}^{\sin 2\phi}$ is small and compatible with zero in the kinematics of HERMES, JLab, and COMPASS [1, 2, 22, 25, 26].

The theoretical description of twist-3 observables is challenging in single-hadron SIDIS. Although lots of effort was devoted to their study [27, 28, 29, 30, 31, 32, 33, 34, 35, 36, 37, 38, 39, 40, 41], these observables are still not understood. Partially, this has to do with the problem of formulating a TMD-factorization at twist-3 level [42, 43].

An important process which can provide independent information on twist-3 TMDs is the

N/q	U	L	T
U	$f^{\perp}$	$g^{\perp}$	h ,e
L	$f_L^{\perp}$	$g_L^{\perp}$	h_L ,e_L
T	f_T , $f_T^{\perp}$	g_T , $g_T^{\perp}$	h_T ,e_T ,$h_T^{\perp}$, $e_T^{\perp}$

Table 1: Twist-3 transverse momentum dependent distribution functions. The U,L,T correspond to unpolarized, longitudinally polarized and transversely polarized nucleons (rows) and quarks (columns)

di-hadron production in SIDIS described by interference functions [44, 45, 46, 47, 48, 49, 50]. In fact, the measurement of single-spin asymmetries with longitudinally polarized target or beam is sensitive in particular to the twist-3 chiral-odd distribution functions e and h_L, in combination with the chiral-odd interference fragmentation function $H_1^{\sphericalangle}$ [48]. This effect survives after integration over quark transverse momenta and can be analyzed in the framework of collinear factorization. The dihadron production becomes a unique tool to study the higher twist effects appearing as $\sin\phi$ modulations in target or beam spin dependent azimuthal moments of the SIDIS cross section. The interference fragmentation function $H_1^{\sphericalangle}$ has been used to obtain information on the transversity parton distribution function [51].

One of the main sources of systematic uncertainties is the contribution from target fragmentation, which is of its own interest and will be also studied in proposed measurement. It was shown that the leading order azimuthal asymmetries in case one of the hadrons is produced in the target fragmentation region provide access to polarized TMD Fracture Functions, which are conditional probabilities to produce a hadron h in TFR when hard scattering occurs on quark q from the target nucleon N. For these processes for longitudinally polarized lepton scattering, the cross-section depends on initial quark longitudinal polarization even if one does not measure the final quark polarization already in leading order.

The JLab 12-GeV upgrade will provide the unique combination of wide kinematic coverage, high beam intensity (luminosity), high energy, high polarization, and advanced detection capabilities necessary to study the transverse momentum and spin correlations in di-hadron production in double-polarized semi-inclusive processes both in the target and current fragmentation regions.

2 Dihadron production in the current fragmentation region

We consider the process

$$\ell(l) + N(P) \to \ell(l') + h_1(P_1) + h_2(P_2) + X, \tag{1}$$

where ℓ denotes the beam lepton, N the nucleon target, and h the produced hadron, and where four-momenta are given in parentheses.

In the one-photon exchange approximation and neglecting the lepton mass, the cross section for two-particle inclusive DIS can be written in the following way [52].

$$\frac{d\sigma}{dx\,dy\,d\psi\,dz\,d\phi_R\,dM_h^2\,d\cos\theta} =$$
$$\frac{\alpha^2}{xy\,Q^2}\,\frac{y^2}{2\,(1-\varepsilon)}\left(1+\frac{\gamma^2}{2x}\right)\Bigg\{F_{UU,T}+\varepsilon\,F_{UU,L}+\sqrt{2\,\varepsilon(1+\varepsilon)}\,\cos\phi_R\,F_{UU}^{\cos\phi_R}$$
$$+\,\varepsilon\cos(2\phi_R)\,F_{UU}^{\cos 2\phi_R}+\lambda_e\,\sqrt{2\,\varepsilon(1-\varepsilon)}\,\sin\phi_R\,F_{LU}^{\sin\phi_R}$$
$$+\,S_L\left[\sqrt{2\,\varepsilon(1+\varepsilon)}\,\sin\phi_R\,F_{UL}^{\sin\phi_R}+\varepsilon\sin(2\phi_R)\,F_{UL}^{\sin 2\phi_R}\right]$$
$$+\,S_L\lambda_e\left[\sqrt{1-\varepsilon^2}\,F_{LL}+\sqrt{2\,\varepsilon(1-\varepsilon)}\,\cos\phi_R\,F_{LL}^{\cos\phi_R}\right]$$
$$+\,|\boldsymbol{S}_T|\left[\sin(\phi_R-\phi_S)\left(F_{UT,T}^{\sin(\phi_R-\phi_S)}+\varepsilon\,F_{UT,L}^{\sin(\phi_R-\phi_S)}\right)\right.$$
$$+\,\varepsilon\,\sin(\phi_R+\phi_S)\,F_{UT}^{\sin(\phi_R+\phi_S)}+\varepsilon\,\sin(3\phi_R-\phi_S)\,F_{UT}^{\sin(3\phi_R-\phi_S)}$$
$$\left.+\,\sqrt{2\,\varepsilon(1+\varepsilon)}\,\sin\phi_S\,F_{UT}^{\sin\phi_S}+\sqrt{2\,\varepsilon(1+\varepsilon)}\,\sin(2\phi_R-\phi_S)\,F_{UT}^{\sin(2\phi_R-\phi_S)}\right]$$
$$+\,|\boldsymbol{S}_T|\lambda_e\left[\sqrt{1-\varepsilon^2}\,\cos(\phi_R-\phi_S)\,F_{LT}^{\cos(\phi_R-\phi_S)}+\sqrt{2\,\varepsilon(1-\varepsilon)}\,\cos\phi_S\,F_{LT}^{\cos\phi_S}\right.$$
$$\left.+\,\sqrt{2\,\varepsilon(1-\varepsilon)}\,\cos(2\phi_R-\phi_S)\,F_{LT}^{\cos(2\phi_R-\phi_S)}\right]\Bigg\}, \qquad (2)$$

where α is the fine structure constant, λ_e is the beam polarization, M_1, M_2 and P_1, P_2 masses and momenta of final hadrons, respectively. Following the Trento conventions [53] all relevant angles are defined on Fig. 1 [54].[1] The final hadrons invariant mass M_h is assumed to be much smaller than the hard scale $Q^2 = -q^2 \geq 0$ ($q = l - l'$) of the SIDIS process defined by kinematic variables $x = Q^2/2\,P\cdot q$, $y = P\cdot q/P\cdot l$, $z = P\cdot P_h/P\cdot q$, $\gamma = 2Mx/Q$. The $P_h = P_1 + P_2$ and $R = (P_1 - P_2)/2$ are the pair total momentum and relative momentum, respectively.

In the center-of-mass (cm) frame of the two hadrons, the emission occurs back-to-back and the key variable is the polar angle θ between the directions of the emission and of P_h in the photon-target rest frame.

The structure functions on the r.h.s. depend on x, Q^2, z, $\cos\theta$, M_h^2. The angle ψ is the azimuthal angle of ℓ' around the lepton beam axis with respect to an arbitrary fixed direction, which in case of a transversely polarized target we choose to be the direction of S. The corresponding relation between ψ and ϕ_S is given in Ref. [55]; in deep inelastic kinematics

[1] From the theoretical point of view, different definitions for the azimuthal angles may be adopted, as long as they differ by terms of order γ^2.

one has $d\psi \approx d\phi_S$. The first and second subscript of the above structure functions indicate the respective polarization of beam and target, whereas the third subscript in $F_{UU,T}$, $F_{UU,L}$ and $F_{UT,T}^{\sin(\phi_h-\phi_S)}$, $F_{UT,L}^{\sin(\phi_h-\phi_S)}$ specifies the polarization of the virtual photon. The longitudinal or transverse target polarization refer to the photon direction here. The ratio ε of longitudinal and transverse photon flux in (2) is given by [52]

$$\varepsilon = \frac{1 - y - \frac{1}{4}\gamma^2 y^2}{1 - y + \frac{1}{2}y^2 + \frac{1}{4}\gamma^2 y^2}, \tag{3}$$

The conversion to the experimentally relevant longitudinal or transverse polarization w.r.t. the lepton beam direction is straightforward and given in [55]. It turns out that measurements with longitudinally polarized targets along the beam receive small contributions from the structure functions with transverse polarization w.r.t. the photon. Single-hadron measurements indicate that this contribution is usually negligible. This issue will be considered with care in our analysis. For the moment, we restrict our attention only to the longitudinal structure functions.

The relevant spin asymmetries can be built as ratios of structure functions. For the longitudinal polarization of the beam or of the target, alternatively, i.e. on the LU and UL combinations one can define the following asymmetries:

$$\begin{aligned}
A_{LU}^{\sin\phi_R \sin\theta}(x, y, z, M_h, Q) &= \frac{1}{\lambda_e} \frac{\frac{8}{\pi}\int d\phi_R \; d\cos\theta \;\; \sin\phi_R \, (d\sigma^+ - d\sigma^-)}{\int d\phi_R \; d\cos\theta \, (d\sigma^+ + d\sigma^-)} = \frac{\frac{4}{\pi}\sqrt{2\,\varepsilon(1-\varepsilon)}\int d\cos\theta \, F_{LU}^{\sin\phi_R}}{\int d\cos\theta \;\; (F_{UU,T} + \epsilon F_{UU,L})}, \\
A_{UL}^{\sin\phi_R \sin\theta}(x, y, z, M_h, Q) &= \frac{1}{S_L} \frac{\frac{8}{\pi}\int d\phi_R \; d\cos\theta \;\; \sin\phi_R \, (d\sigma^+ - d\sigma^-)}{\int d\phi_R \; d\cos\theta \, (d\sigma^+ + d\sigma^-)} = \frac{\frac{4}{\pi}\sqrt{2\,\varepsilon(1+\varepsilon)}\int d\cos\theta \, F_{UL}^{\sin\phi_R}}{\int d\cos\theta \;\; (F_{UU,T} + \epsilon F_{UU,L})}.
\end{aligned} \tag{4}$$

In the limit $M_h^2 \ll Q^2$ the structure functions can be written in terms of PDF and Dihadron Fragmentation Functions (DiFF) in the following way (a summation $\sum_q e_q^2$ is

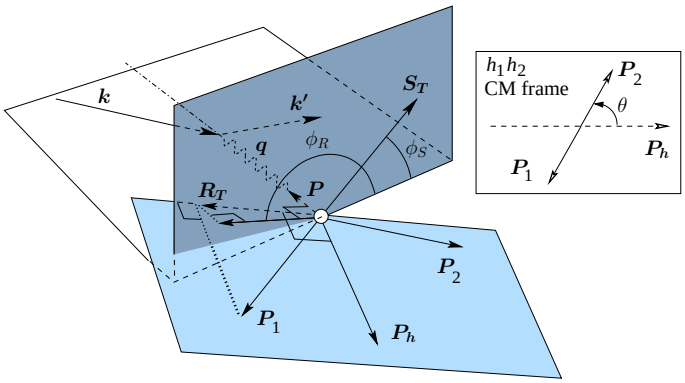

Figure 1: Depiction of the azimuthal angles ϕ_R of the dihadron and ϕ_S of the component $\boldsymbol{S_T}$ of the target-polarization transverse to both the virtual-photon and target-nucleon momenta $\boldsymbol{q}$ and $\boldsymbol{P}$, respectively. Both angles are evaluated in the virtual-photon-nucleon center-of-momentum frame. Explicitly, $\phi_R \equiv \frac{(\boldsymbol{q}\times\boldsymbol{k})\cdot\boldsymbol{R_T}}{|(\boldsymbol{q}\times\boldsymbol{k})\cdot\boldsymbol{R_T}|}\arccos\frac{(\boldsymbol{q}\times\boldsymbol{k})\cdot(\boldsymbol{q}\times\boldsymbol{R_T})}{|\boldsymbol{q}\times\boldsymbol{k}||\boldsymbol{q}\times\boldsymbol{R_T}|}$ and $\phi_S \equiv \frac{(\boldsymbol{q}\times\boldsymbol{k})\cdot\boldsymbol{S_T}}{|(\boldsymbol{q}\times\boldsymbol{k})\cdot\boldsymbol{S_T}|}\arccos\frac{(\boldsymbol{q}\times\boldsymbol{k})\cdot(\boldsymbol{q}\times\boldsymbol{S_T})}{|\boldsymbol{q}\times\boldsymbol{k}||\boldsymbol{q}\times\boldsymbol{S_T}|}$. Here, $\boldsymbol{R_T} = \boldsymbol{R} - (\boldsymbol{R}\cdot\hat{\boldsymbol{P_h}})\hat{\boldsymbol{P_h}}$, with $\boldsymbol{R} \equiv (\boldsymbol{P_1} - \boldsymbol{P_2})/2$, $\boldsymbol{P_h} \equiv \boldsymbol{P_1} + \boldsymbol{P_2}$, and $\hat{\boldsymbol{P_h}} \equiv \boldsymbol{P_h}/\mid \boldsymbol{P_h} \mid$, thus R_T is the component of P_1 orthogonal to P_h, and $\phi_{R\perp}$ is the azimuthal angle of R_T about the virtual-photon direction. The dotted lines indicate how vectors are projected onto planes. The short dotted line is parallel to the direction of the virtual photon. Also included is a description of the polar angle θ, which is defined as the angle between the direction of P_1 in the hadron pair center-of-mass frame, and the direction of P_h in the photon-target rest frame.

understood) [48][2]

$$F_{UU,T} = x f_1^q(x)\, D_1^q\big(z, \cos\theta, M_h\big), \tag{5}$$

$$F_{UU,L} = 0, \tag{6}$$

$$F_{UU}^{\cos\phi_R} = -x\frac{|\boldsymbol{R}|\sin\theta}{Q}\,\frac{1}{z}\,f_1^q(x)\,\widetilde{D}^{\sphericalangle q}\big(z, \cos\theta, M_h\big), \tag{7}$$

$$F_{UU}^{\cos 2\phi_R} = 0, \tag{8}$$

$$F_{LU}^{\sin\phi_R} = -x\frac{|\boldsymbol{R}|\sin\theta}{Q}\left[\frac{M}{M_h}\,x\,e^q(x)\,H_1^{\sphericalangle q}\big(z, \cos\theta, M_h\big) + \frac{1}{z}\,f_1^q(x)\,\widetilde{G}^{\sphericalangle q}\big(z, \cos\theta, M_h\big)\right], \tag{9}$$

$$F_{UL}^{\sin\phi_R} = -x\frac{|\boldsymbol{R}|\sin\theta}{Q}\left[\frac{M}{M_h}\,x\,h_L^q(x)\,H_1^{\sphericalangle q}\big(z, \cos\theta, M_h\big) + \frac{1}{z}\,g_1^q(x)\,\widetilde{G}^{\sphericalangle q}\big(z, \cos\theta, M_h\big)\right], \tag{10}$$

$$F_{UL}^{\sin 2\phi_R} = 0, \tag{11}$$

$$F_{LL} = x g_1^q(x)\, D_1^q\big(z, \cos\theta, M_h\big), \tag{12}$$

$$F_{LL}^{\cos\phi_R} = -x\frac{|\boldsymbol{R}|\sin\theta}{Q}\,\frac{1}{z}\,g_1^q(x)\,\widetilde{D}^{\sphericalangle q}\big(z, \cos\theta, M_h\big), \tag{13}$$

[2]For some discussion of the case $M_h^2 \approx Q^2$, see Ref. [56]

where

$$|\boldsymbol{R}| = \frac{1}{2}\sqrt{M_h^2 - 2(M_1^2 + M_2^2) + (M_1^2 - M_2^2)^2/M_h^2}. \tag{14}$$

All the structure functions that vanish can be nonzero at order $\mathcal{O}\Big(\frac{M^2}{Q^2}, \frac{M_h^2}{Q^2}\Big)$.

In the above structure functions, there are essentially three kinds of combinations of PDF and fragmentation functions (FF):[3] leading-twist PDF and FF (e.g., $f_1 D_1$), leading-twist PDF and subleading-twist FF (e.g., $f_1 \widetilde{D}^{\sphericalangle}$), subleading-twist PDF and leading-twist FF (e.g., $e H_1^{\sphericalangle}$).

The main interest of the structure functions with leading-twist combinations ($F_{UU,T}$ in particular) is to allow a flavor-dependent analysis of the DiFF D_1, similarly to what happens for the single-hadron case.

The subleading-twist fragmentation functions $\widetilde{D}^{\sphericalangle}$ and $\widetilde{G}^{\sphericalangle}$ originate from quark-gluon correlation functions on the fragmentation side. They vanish in the so-called Wandzura–Wilczek approximation [57]. Although this approximation is often used in phenomenological works (see, e.g., [58, 59, 60, 61] and references therein) there are no compelling theoretical grounds for supporting its validity [62, 63, 64, 65]. At present it is not confirmed nor disapproved by experimental data [65]. The measurement of $\cos\phi_R$ modulations in unpolarized or doubly polarized collisions ($F_{UU}^{\cos\phi_R}$ and $F_{LL}^{\cos\phi_R}$) offers a way to address this question directly and represents an example of how dihadron measurements can be useful for the study of quark-gluon correlations in general.

The most interesting terms for our purposes are the ones containing the functions e and h_L, multiplied by the interference fragmentation function $H_1^{\sphericalangle}$, occurring in the structure functions $F_{LU}^{\sin\phi_R}$ and $F_{UL}^{\sin\phi_R}$. The extraction of the PDF is made possible by the fact that $H_1^{\sphericalangle}$ has been recently extracted [51] from BELLE measurements [14]. Unfortunately, the structure functions contain also another term involving the fragmentation function $\widetilde{G}^{\sphericalangle}$. The possibilities to isolate the crucial quantities are the following: (i) rely on the measurements of the function $\widetilde{G}^{\sphericalangle}$ from e^+e^- collisions, (ii) rely on the knowledge of the leading-twist PDF f_1 and g_1 and build combinations of the structure functions where only the interesting terms survive. The latter option will be discussed later in a particular case.

Two other contributions to the structure functions $F_{UU}^{\cos\phi_R}$ and $F_{LL}^{\cos\phi_R}$, included in Ref. [48], contain the collinear T-odd distribution functions h and e_L. They should vanish if the gauge link is the only source of a T-odd behavior. Measuring a nonzero h or e_L would cast doubts on collinear factorization at subleading twist. It would be interesting to experimentally check this feature, even though the problem is complicated by the presence of the standard T-even terms discussed above. The significance of such an observation can be compared to the measurements of a nonzero $\sin\phi_S$ signal in inclusive DIS [66, 67, 68, 69], which indicates either a violation of T-reversal invariance or the presence of a significant two-photon exchange contribution [70].

[3] leading-twist functions are always indicated by a subscript 1

2.1 Partial-wave analysis

Two-hadron fragmentation functions can be decomposed in partial waves in the following way [47]:

$$D_1 \to D_{1,ss+pp} + D_{1,sp}\cos\theta + D_{1,pp}\frac{1}{4}\left(3\cos^2\theta - 1\right) , \tag{15}$$

$$H_1^{\sphericalangle} \to H_{1,sp}^{\sphericalangle} + H_{1,pp}^{\sphericalangle}\cos\theta . \tag{16}$$

$$\widetilde{D}^{\sphericalangle} \to \widetilde{D}_{sp}^{\sphericalangle} + \widetilde{D}_{pp}^{\sphericalangle}\cos\theta , \tag{17}$$

$$\widetilde{G}^{\sphericalangle} \to \widetilde{G}_{sp}^{\sphericalangle} + \widetilde{G}_{pp}^{\sphericalangle}\cos\theta , \tag{18}$$

$$\tag{19}$$

where the relative partial waves of each pion pair are put into evidence. For sake of simplicity, we will make the replacement $D_{1,ss+pp} \equiv D_1$ since no ambiguity arises in the following.

The functions on the r.h.s. depend on z, M_h. It may be useful to note that a symmetrization $f(\theta) + f(\pi - \theta)$ gets rid of all the $\cos\theta$ terms [54]. In general, those terms will vanish even if the θ acceptance is not complete but still symmetric about $\theta = \pi/2$.

A thorough study of the cross section with partial-wave analysis has been recently presented in Ref. [71], with a different notation compared to the one adopted here.

2.2 Flavor structure

We now discuss the flavor structure of the structure functions. The analysis will be different depending on the kind of target and final-state hadrons. We will consider here $\pi^+\pi^-$, K^+K^-, or $K^+\pi^-$ final-state pairs.

Isospin symmetry and charge conjugation suggest the relations [51]

$$D_1^{u\to\pi^+\pi^-} = D_1^{d\to\pi^+\pi^-} = D_1^{\bar{u}\to\pi^+\pi^-} = D_1^{\bar{d}\to\pi^+\pi^-} , \tag{20}$$

$$D_1^{s\to\pi^+\pi^-} = D_1^{\bar{s}\to\pi^+\pi^-} , \tag{21}$$

$$D_1^{c\to\pi^+\pi^-} = D_1^{\bar{c}\to\pi^+\pi^-} , \tag{22}$$

$$H_1^{\sphericalangle u\to\pi^+\pi^-} = -H_1^{\sphericalangle d\to\pi^+\pi^-} = -H_1^{\sphericalangle \bar{u}\to\pi^+\pi^-} = H_1^{\sphericalangle \bar{d}\to\pi^+\pi^-} , \tag{23}$$

$$H_1^{\sphericalangle s\to\pi^+\pi^-} = -H_1^{\sphericalangle \bar{s}\to\pi^+\pi^-} = H_1^{\sphericalangle c\to\pi^+\pi^-} = -H_1^{\sphericalangle \bar{c}\to\pi^+\pi^-} = 0 . \tag{24}$$

For $\tilde{G}^{\sphericalangle}$ we expect the same relations as for $H_1^{\sphericalangle}$. In practice, for $\pi^+\pi^-$ and neglecting charm quarks, there are only two independent D_1 functions and one $H_1^{\sphericalangle}$ (and $\tilde{G}^{\sphericalangle}$).

For K^+K^-, similar considerations lead to

$$D_1^{u\to K^+K^-} = D_1^{\bar{u}\to K^+K^-}, \tag{25}$$
$$D_1^{s\to K^+K^-} = D_1^{\bar{s}\to K^+K^-}, \tag{26}$$
$$D_1^{d\to K^+K^-} = D_1^{\bar{d}\to K^+K^-}, \tag{27}$$
$$D_1^{c\to K^+K^-} = D_1^{\bar{c}\to K^+K^-}, \tag{28}$$
$$H_1^{\sphericalangle u\to K^+K^-} = -H_1^{\sphericalangle \bar{u}\to K^+K^-} \tag{29}$$
$$H_1^{\sphericalangle s\to K^+K^-} = -H_1^{\sphericalangle \bar{s}\to K^+K^-}, \tag{30}$$
$$H_1^{\sphericalangle d\to K^+K^-} = -H_1^{\sphericalangle \bar{d}\to K^+K^-} = H_1^{\sphericalangle c\to K^+K^-} = -H_1^{\sphericalangle \bar{c}\to K^+K^-} = 0\,. \tag{31}$$

For K^+K^- and neglecting charm quarks, there are three independent D_1 functions and two $H_1^{\sphericalangle}$.

The flavor structure of $K^+\pi^-$ suggests

$$D_1^{u\to K^+\pi^-} = D_1^{\bar{u}\to K^+\pi^-} \tag{32}$$
$$D_1^{s\to K^+\pi^-} = D_1^{\bar{d}\to K^+\pi^-} = D_1^{c\to K^+\pi^-} = D_1^{\bar{c}\to K^+\pi^-}, \tag{33}$$
$$H_1^{\sphericalangle u\to K^+\pi^-} = -H_1^{\sphericalangle \bar{u}\to K^+\pi^-} \tag{34}$$
$$H_1^{\sphericalangle s\to K^+\pi^-} = H_1^{\sphericalangle \bar{d}\to K^+\pi^-} = H_1^{\sphericalangle c\to K^+\pi^-} = H_1^{\sphericalangle \bar{c}\to K^+\pi^-} = 0\,. \tag{35}$$

Together with the above functions, we have to consider also $D_1^{d\to K^+\pi^-}$ and $D_1^{\bar{s}\to K^+\pi^-}$, for a total of four independent unpolarized fragmentation functions, and $H_1^{\sphericalangle d\to K^+\pi^-}$ and $H_1^{\sphericalangle \bar{s}\to K^+\pi^-}$, for a total of three independent interference fragmentation functions.

2.3 Observables

Using the expressions of the structure functions (9), and (10), which are valid up to corrections of order M^2/Q^2, and the partial-wave expansion of the fragmentation functions in Sec. 2.1, we can rewrite the asymmetries of Eqs. (4) as

$$A_{LU}^{\sin\phi_R\sin\theta}(x,y,z,M_h,Q) = -\frac{W(y)}{A(y)}\,\frac{M}{Q}\,\frac{|\boldsymbol{R}|}{M_h}\,\frac{\sum_q e_q^2\left[x e^q(x)\,H_{1,sp}^{\sphericalangle,q}(z,M_h) + \frac{M_h}{zM}\,f_1^q(x)\,\tilde{G}_{sp}^{\sphericalangle,q}(z,M_h)\right]}{\sum_q e_q^2\,f_1^q(x)\,D_{1,ss+pp}^q(z,M_h)}\,, \tag{36}$$

$$A_{UL}^{\sin\phi_R\sin\theta}(x,y,z,M_h,Q) = -\frac{V(y)}{A(y)}\,\frac{M}{Q}\,\frac{|\boldsymbol{R}|}{M_h}\,\frac{\sum_q e_q^2\left[x h_L^q(x)\,H_{1,sp}^{\sphericalangle,q}(z,M_h) + \frac{M_h}{zM}\,g_1^q(x)\,\tilde{G}_{sp}^{\sphericalangle,q}(z,M_h)\right]}{\sum_q e_q^2\,f_1^q(x)\,D_{1,ss+pp}^q(z,M_h)}\,. \tag{37}$$

The kinematical factors $W(y), V(y)$ and $A(y)$ are defined in the Eq.2 (see Appendix-A 9). For the specific case of the $\pi^+\pi^-$ final state, we can introduce in the flavor sum the

assumptions (20)–(24), and we get

$$A_{LU}^{\sin\phi_R \sin\theta}(x,y,z,M_h,Q) \approx -\frac{W(y)}{A(y)}\,\frac{M}{Q}\,\frac{|\boldsymbol{R}|}{M_h} \times \frac{H_{1,sp}^{\sphericalangle,u}\left[4xe^{u-\bar{u}}(x)-xe^{d-\bar{d}}(x)\right]+\frac{M_h}{zM}\,\tilde{G}_{sp}^{\sphericalangle,u}\left[4xf_1^{u-\bar{u}}(x)-xf_1^{d-\bar{d}}(x)\right]}{D_1^u\left[4f_1^{u+\bar{u}}(x)+f_1^{d+\bar{d}}(x)\right]+D_1^s\,f_1^{s+\bar{s}}(x)}\,, \tag{38}$$

$$A_{UL}^{\sin\phi_R \sin\theta}(x,y,z,M_h,Q) \approx -\frac{V(y)}{A(y)}\,\frac{M}{Q}\,\frac{|\boldsymbol{R}|}{M_h} \times \frac{H_{1,sp}^{\sphericalangle,u}\left[4xh_L^{u-\bar{u}}(x)-xh_L^{d-\bar{d}}(x)\right]+\frac{M_h}{zM}\,\tilde{G}_{sp}^{\sphericalangle,u}\left[4xg_1^{u-\bar{u}}(x)-xg_1^{d-\bar{d}}(x)\right]}{D_1^u\left[4f_1^{u+\bar{u}}(x)+f_1^{d+\bar{d}}(x)\right]+D_1^s\,f_1^{s+\bar{s}}(x)}\,, \tag{39}$$

where for the PDF we adopt the compact notation $f_1^{q\pm\bar{q}}(x) = f_1^q(x) \pm f_1^{\bar{q}}(x)$, and similarly for the other functions. For neutron targets, assuming isospin symmetry, we can simply interchange the role of u and d quarks in the PDF.

We can work out this example at a deeper level and build a new observable that is independent of the unknown function $\tilde{G}^{\sphericalangle}$. In fact, the following combination of asymmetries reads

$$\begin{aligned} A_{ULU}^{\sin\phi_R \sin\theta}(x,y,z,M_h,Q) &= A_{UL}^{\sin\phi_R \sin\theta}\,\frac{1}{4g_1^{u-\bar{u}}(x)-g_1^{d-\bar{d}}(x)} - A_{LU}^{\sin\phi_R \sin\theta}\,\frac{1}{4f_1^{u-\bar{u}}(x)-f_1^{d-\bar{d}}(x)} \\ &= \frac{M}{Q}\,\frac{1}{2}\sqrt{1-4\frac{m_\pi^2}{M_h^2}}\,\frac{xH_{1,sp}^{\sphericalangle,u}(z,M_h)}{D_1^u(z,M_h)\left[4f_1^{u+\bar{u}}(x)+f_1^{d+\bar{d}}(x)\right]+D_1^s(z,M_h)\,f_1^{s+\bar{s}}(x)} \\ &\quad\times\left\{\frac{W(y)}{A(y)}\,\frac{4e^{u-\bar{u}}(x)-e^{d-\bar{d}}(x)}{4f_1^{u-\bar{u}}(x)-f_1^{d-\bar{d}}(x)} - \frac{V(y)}{A(y)}\,\frac{4h_L^{u-\bar{u}}(x)-h_L^{d-\bar{d}}(x)}{4g_1^{u-\bar{u}}(x)-g_1^{d-\bar{d}}(x)}\right\}\,. \end{aligned} \tag{40}$$

2.4 Parametrization of DiFF

The chiral-odd Dihadron Fragmentation Function $H_1^{\sphericalangle q}$ [46] describes the correlation between the transverse polarization of the fragmenting quark with flavor q and the azimuthal orientation of the plane containing the momenta of the detected hadron pair. $H_{1,sp}^{\sphericalangle q}$ is the component of $H_1^{\sphericalangle q}$ that is sensitive to the interference between the fragmentation amplitudes into pion pairs in relative s wave and in relative p wave, from which comes the common name of Interference Fragmentation Functions [44]. For this reason, we expect the function to be sizeable in kinematic regions where s and p waves are present. This is typically true where spin-1 resonances (e.g., ρ or K^*) are present.

Before the Belle measurement of the angular distribution of two pion pairs in e^+e^- annihilation [14], the only estimates of DiFF were based on model calculations [72, 46, 49].

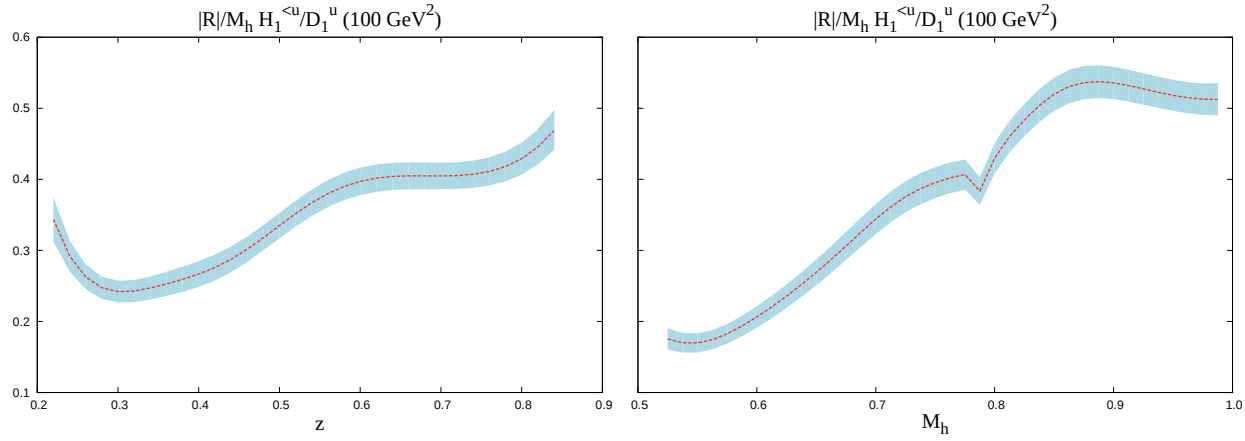

Figure 2: The ratio $|\boldsymbol{R}|H_{1,sp}^{\sphericalangle,u}/M_h D_1^u$ as a function of z and M_h respectively. The error band comes from the calculation of error propagation from the fit.

The unpolarized D_1 was tuned to Monte Carlo event generators [49] and the polarized $H_{1,sp}^{\sphericalangle}$ compared to HERMES asymmetry data [73].

The recent analyze of the so-called Artru–Collins asymmetry [74] by the Belle collaboration gave rise to new parametrization of both D_1 and $H_{1,sp}^{\sphericalangle}$ for the production of $\pi^+\pi^-$.

The former was parametrized to reproduce the two-hadron yields of the PHYTIA event generator, which is known to give a good description of data. Three main decay channels were considered for $\pi^+\pi^-$: (i) ρ resonance decaying into the two pions, (ii) ω resonance decaying into the two pions, plus the fragmentation into a ω resonance decaying into $\pi^+\pi^-\pi^0$ with π^0 unobserved, (iii) the continuum, i.e. the fragmentation into an "incoherent" $\pi^+\pi^-$ pair. Combining the fit of the asymmetry data with the parametrization of its denominator allowed the extraction of the IFF $H_{1,sp}^{\sphericalangle}$.

The ratio $|\boldsymbol{R}|H_{1,sp}^{\sphericalangle,u}(z,M_h)/M_h D_1^u(z,M_h)$ at the Belle's scale is depicted in Fig. 2. It is integrated over M_h or z, respectively. The error band is estimated through the propagation of errors based on the fit's results. The evolution effects, downward to HERMES' scale, have been studied in Ref. [51]. The integrals of DiFF over the kinematical ranges for (z, M_h) at both scales lead to the ratios

$$\frac{n^u_{H_1^{\sphericalangle}}}{n^u_{D_1}}(\sim 2\ \mathrm{GeV}^2)\Big/\frac{n^u_{H_1^{\sphericalangle}}}{n^u_{D_1}}(100\ \mathrm{GeV}^2) = 92\% \pm 8\%, \quad . \tag{41}$$

indicating that evolution effects are almost negligible at the level of integrated DiFF. We will not take such a correction into account in this proposal.

There is at the moment no data on interference fragmentation functions for $K\pi$ pairs. In order to have an estimate of the magnitude of the effect, we assume it to have this form

$$\frac{|\boldsymbol{R}|H_{1,sp}^{\sphericalangle}(z,M_h)}{M_h D_1(z,M_h)} \approx 3M_h \frac{|\boldsymbol{R}|\sqrt{D_{1\mathrm{con}}(z,M_h)\, D_{1K^*}(z,M_h)}}{M_h D_1(z,M_h)} \tag{42}$$

where with $D_{1\mathrm{con}}$ and D_{1K^*} we mean the components of the fragmentation function that describe the $K\pi$ continuum and the K^* resonance, respectively. We estimate these fragmentation function components using the LEPTO Monte Carlo event generator. The above

ansatz is motivated by the fact that the function $H_{1,sp}^{\sphericalangle}$ arises from the interference between pairs produced in s wave and p wave (as explained at the beginning of the section). The above ansatz applied to the $\pi^+\pi^-$ system reproduces the size and qualitative feature of the extracted ratio displayed in Fig. 2. Finally, for $K\pi$ pairs we assume that the fragmentation function is the same for all flavors (the largest component should anyway come from the u quark).

2.5 The parton distribution functions e and h_L

The PDFs $e(x)$ and $h_L(x)$ are twist-3 functions which can be written in the following way [75, 52]

$$xe = x\tilde{e} + \frac{m}{M} f_1, \tag{43}$$

$$xh_L = x\tilde{h}_L + \frac{p_T^2}{M^2} h_{1L}^{\perp} + \frac{m}{M} g_{1L}. \tag{44}$$

The functions on the l.h.s. can be expressed in terms of quark fields only. This property allows an explicit calculation in quark models [76]. The functions with the tilde on the r.h.s. are related to quark-gluon-quark correlators and are specifically referred to as "pure twist-3" contributions [62]. The rest of each expression on the r.h.s. contains only twist-2 functions and corresponds to its Wandzura–Wilczek part. Neglecting quark masses, the function $xe(x)$ is entirely determined by pure twist-3 contributions. (Notice that multiplying $e(x)$ by x is necessary to cancel a δ-function-type singularity at $x = 0$, see below.)

The function $e(x)$ has attracted a lot of interest [37] because it is directly related to the soft physics of chiral symmetry breaking [77].

The first Mellin moment of the isoscalar flavor-combination of $e^a(x)$ is related to the pion-nucleon sigma-term

$$\int_0^1 dx\, (e^u + e^{\bar{u}} + e^d + e^{\bar{d}})(x) = \frac{\sigma_{\pi N}}{m} \tag{45}$$

where $m = \frac{1}{2}(m_u + m_d)$ is the average current mass of light quarks, and (small) "double-isospin-breaking" effects proportional to $(m_u - m_d)\langle N|(\bar{\psi}_u\psi_u - \bar{\psi}_d\psi_d)|N\rangle$ are neglected. In the pre-QCD era $\sigma_{\pi N}$ was introduced as the double commutator of the strong interaction Hamiltonian with two axial isovector charges [78]. In QCD it is related to matrix elements of the operators $m_q\bar{\psi}_q\psi_q$ which explicitly break chiral symmetry. In the chiral limit $\sigma_{\pi N} \to 0$ but $\sigma_{\pi N}/m$ is finite. The pion-nucleon sigma-term is given by the scalar form factor $\sigma(t)$ at zero momentum transfer $t = 0$. This form factor describes the elastic scattering off a spin-$\frac{1}{2}$ target via the exchange of a spin-0 particle (e.g. the Higgs [79]), and has not yet been measured except for its value in the time-like region at the so-called Chen-Dashen point $t = 2m_\pi^2$, with m_π the pion mass, which can be deduced from pion-nucleon scattering data by means of low-energy theorems [80, 81, 82]. Chiral perturbation theory and dispersion relation technics allow to relate $\sigma(2m_\pi^2)$ to $\sigma(0) \equiv \sigma_{\pi N}$ [83, 84, 85]. The phenomenological

value of $\sigma_{\pi N}$ =(50-70 MeV) [83, 86, 87, 88] is sometimes said to be "unexpectedly large" because it implies a large "strangeness content of the nucleon" defined as

$$y_N = \frac{\langle N|\bar{\psi}_s\psi_s|N\rangle}{\frac{1}{2}\langle N|(\bar{\psi}_u\psi_u + \bar{\psi}_d\psi_d)N\rangle} = 1 - \frac{m}{m_s - m}\,\frac{M_\Xi + M_\Sigma - 2M_N}{\sigma_{\pi N}} \tag{46}$$

where the second equality is valid in leading order of chiral perturbation theory [89, 90]. Numerically one finds y_N =0.2–0.4 but this does not imply that (20–40)% of the nucleon mass is due to strangeness (taking also the contributions of the "kinetic" and "potential" energies in QCD into account one deduces a much smaller strangeness contribution to the nucleon mass [91]). Direct lattice studies of $\sigma_{\pi N}$ have been performed [92] but are demanding because of difficulties associated with the renormalization of the operator $m_q\bar{\psi}_q\psi_q$ on the lattice. Another method to deduce $\sigma_{\pi N}$ from lattice calculations makes use of the Feynam-Hallmann theorem [93, 94] which relates $\sigma_{\pi N}$ to the slope of the nucleon mass as function of the pion mass, $\sigma_{\pi N} = m_\pi^2 \frac{\partial M_N}{\partial m_\pi^2}$. Lattice data analysis yield results compatible with the phenomenological $\sigma_{\pi N}$-determinations [95, 96, 97]. Let us also mention the interesting connection of $\sigma_{\pi N}$ to negative Mellin moments of $f_1^a(x)$ discussed in [98]. At first glance, Eq. (45) seems to imply that one could access information on $\sigma_{\pi N}$ from deeply inelastic scattering experiments. But in QCD the contribution of $\sigma_{\pi N}$ to (45) is due to a δ-function-type singularity at $x = 0$, a well-known [99] but rarely emphasized fact [100]. A $\delta(x)$-contribution was found in a (1 + 1)-dimensional version of the Gross-Neveu model [101], in perturbative approaches [102], and in the chiral quark-soliton model [103, 104, 105, 106] (which consistently allows to calculate $\sigma_{\pi N}$ from $\sigma(t)$, the coefficient of $\delta(x)$ in $e(x)$, and the Feynman-Hellmann theorem [107], see also [108]). In the chiral quark-soliton model the origin of the $\delta(x)$-contribution in $e(x)$ is of non-perturbative character [103, 104]. In other models of $e(x)$ no $\delta(x)$-contribution was found [76, 109, 110, 111].

Even though, one cannot access information on $\sigma_{\pi N}$ from DIS measurements of $e(x)$ [100]. Nevertheless, the presence of the $\delta(x)$-singularity in $e(x)$ can be concluded indirectly. Numerically, if the point $x = 0$ was included, the sum rule (45) would give a large number of $\mathcal{O}(10)$ for the first moment of $e(x)$. Experimentally, since the point $x = 0$ cannot be reached, one would observe approximately zero [100]. The possible existence of $\delta(x)$-contributions in structure functions can be inferred from the analytical properties of the respective forward Compton scattering scattering amplitudes and was debated before QCD [112, 113, 114] ($e(x)$ is related to the structure functions $F_4(x)$ and $F_5(x)$ which in principle could be measured in (anti)neutrino-nucleon DIS [113]). More prominent examples of sum rules which could possibly be spoiled in this way are the Burkhardt-Cottingham sum rule [115] and the Gerasimov-Drell-Hearn sum rule [116].

The second moment of $e(x)$ is equally interesting, as it arises from the mass term in (43) suggesting that, in principle, an "extraction" of current quark masses from SIDIS is possible, namely [76]

$$\int_0^1 dx\; x(e^q - e^{\bar{q}})(x) = \frac{m_q}{M_N}\,. \tag{47}$$

But effects associated with $e(x)$ are power suppressed by M_N/Q, i.e. the contribution of (47) to observables is of $\mathcal{O}(m_q/Q)$ and hence negligible. For the above-discussed reasons, the

practical DIS sum rules for $e(x)$ are [100]

$$\int\limits_{\epsilon}^{1} dx\ (e^q + e^{\bar{q}})(x) \approx 0\,, \quad \int\limits_{\epsilon}^{1} dx\ x(e^q - e^{\bar{q}})(x) \approx 0\,, \tag{48}$$

where $\epsilon > 0$ represents the smallest x-value accessible in experiments. This situation is analog to the Efremov-Leader-Teryaev sum rule [117]. The pure twist-3 piece in $e^q(x)$ drops out from the first two moments (45, 47) and contributes only to the third Mellin moment. Noteworthy, the matrix element $\int \mathrm{d}x\, x^2 \tilde{e}^q(x)$ describes the average transverse force acting on a transversely polarized quark q in an unpolarized target after interaction with the virtual photon [24].

The renormalization scale dependence of $\tilde{e}(x)$ and $\tilde{h}_L(x)$ was studied in Refs. [122, 123, 124], see also Refs. [125, 99] for reviews. The evolution of these pure twist-3 functions is characterized by a complicated operator mixing pattern typical for twist-3 quantities. In the multi-color limit the evolution of $\tilde{e}(x)$ simplifies to a DGLAP-type evolution – as it does for the other two nucleon twist-3 distribution functions $\tilde{h}_L(x)$ and (the flavour non-singlet) $\tilde{g}_T(x)$. Figs. 3a and 3b show respectively the evolution of $e^{u+d}(x, Q^2)$ and $e^{\bar{u}+\bar{d}}(x, Q^2)$ from the chiral quark soliton model [103] from an initial scale $\mu_0^2 = (600\,\mathrm{MeV})^2$ of the chiral quark soliton model to higher scales.

In order to better understand the evolution pattern Fig. 3c shows the evolution of the "toy model" $e(x, Q_0^2) = f_1(x, Q_0^2)$ at $Q^2 = 1\,\mathrm{GeV}^2$ to higher scales normalized with respect to $f_1(x, Q^2)$ at the respective scales. The LO unpolarized parton distribution functions at the respective scales are taken from [126]. We see that the ratio of $e(x)/f_1(x)$ drops from unity at $Q_0^2 = 1\,\mathrm{GeV}^2$, by about (20–30) % when going to experimentally relevant scales of typically (2–3) GeV^2 at Jefferson Lab. Finally, Fig. 4 shows the parton distribution functions $e(x)$ and $h_L(x)$ as predicted by the chiral quark soliton model [106, 119] at $Q^2 = 2.5\,\mathrm{GeV}^2$.

These features make $e(x)$ and $h_L(x)$ extremely interesting functions, and having experimental access to them is of great importance.

There are few model calculations concerning the twist-3 PDF: MIT bag model [76, 109, 127], diquark spectator model [110], instanton QCD vacuum calculus [128, 129], chiral quark soliton model [130, 103, 104, 105, 106], and the perturbative light-cone Hamiltonian approach to $\mathcal{O}(\alpha_S)$ with a quark target [102, 111]. In these calculations there are no contributions from either strange or sea quarks, except for the chiral quark soliton model.

The bag model has given several powerful results and predictions concerning PDF as well as transverse-momentum dependent distributions (TMD). It is a relativistic model where quarks and antiquarks are excitations inside the confined bag. It is generally assumed that the proton wave function is invariant under the $SU(6)$ spin-flavor symmetry. In the case of two-body problems, this symmetry leads to proportionality between the different flavor components. The contribution to $e(x)$ in the bag is entirely due to the bag boundary, and therefore to the quark-gluon-quark correlation. The result of the model calculation of the twist-3 $e^u(x)$, $h_L^u(x)$, as well as of the unpolarized distribution $f_1^u(x)$, is depicted in Fig. 5. On the other and, the function $h_L(x)$ contains twist-2 and pure twist-3 contributions. Although it is a popular assumption that pure twist-3 (and mass) terms are small [58, 59, 60, 61], this has rarely been justified by theoretical calculations.

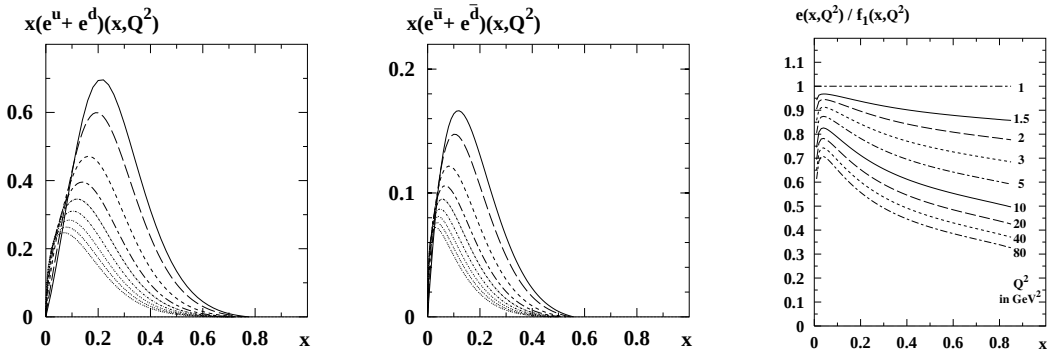

Figure 3: Evolution effects for the isoscalar flavor combinations **(a)** $xe^{u+d}(x)$ and **(b)** $xe^{\bar{u}+\bar{d}}(x)$ from the chiral quark-soliton model in the chiral limit [103]. Solid line: the results at the initial scale of the chiral quark soliton model $\mu_0^2 = (600\,\mathrm{MeV})^2$. The dashed and dotted curves are the results after evolution (in decreasing order) to the scales $Q^2 = 0.5$, 1, 2, 4, 8, 16, 32 and 64 GeV^2. **(c)** The scale dependence of the ratio $e(x,Q^2)/f_1(x,Q^2)$ from the "toy model" $e(x,Q_0^2) = f_1(x,Q_0^2)$ at $Q_0^2 = 1\,\mathrm{GeV}^2$. For definiteness: we use the LO parametrization for $f_1(x,Q^2)$ from [126]. The evolution of $e(x)$ is performed in all figures according to [123].

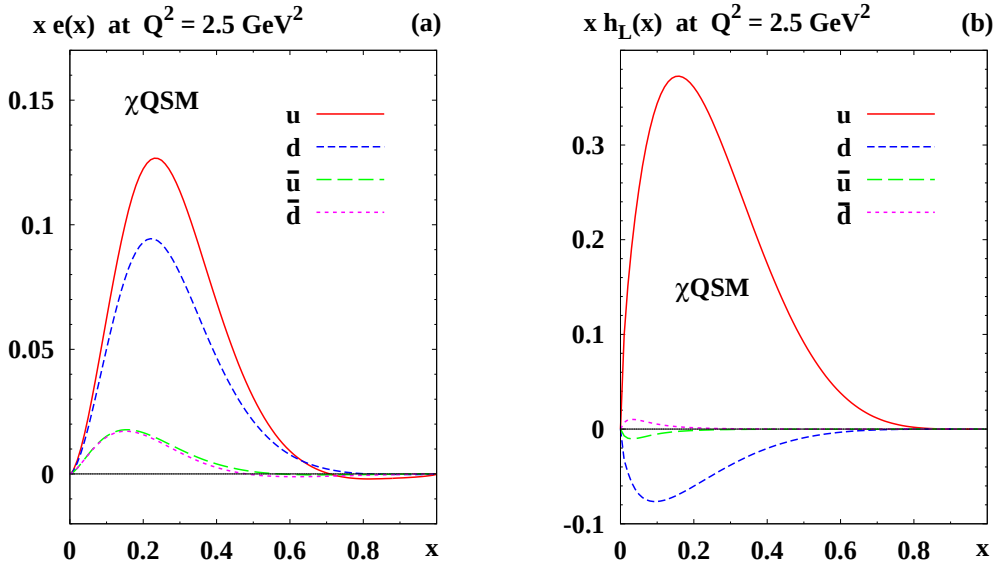

Figure 4: The parton distribution functions $xe(x)$ and $xh_L(x)$ from the chiral quark soliton model (χQSM) [106, 119]. All results are LO-evolved to $Q^2 = 2.5\,\mathrm{GeV}^2$.

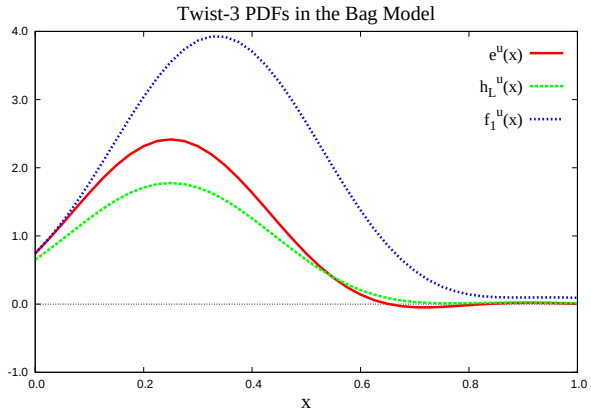

Figure 5: The functions $e^u(x)$, $h_L^u(x)$, and $f_1^u(x)$ in the bag model [76].

In the bag model and assuming for simplicity $\tilde{G}^{\sphericalangle} = 0$, the asymmetries (39) become

$$A_{LU}^{\sin\phi_R \sin\theta}(x, y, z, M_h, Q) = -\frac{W(y)}{A(y)} \frac{M}{Q} \frac{|\boldsymbol{R}|}{M_h} \frac{\left(4 - \frac{1}{2}\right) x e^u(x)\, H_{1,sp}^{\sphericalangle,u}(z, M_h)}{\left(4 + \frac{1}{2}\right) f_1^u(x)\, D_1^u(z, M_h)} \quad , \tag{49}$$

$$A_{UL}^{\sin\phi_R \sin\theta}(x, y, z, M_h, Q) = -\frac{V(y)}{A(y)} \frac{M}{Q} \frac{|\boldsymbol{R}|}{M_h} \frac{\left(4 + \frac{1}{4}\right) x h_L^u(x)\, H_{1,sp}^{\sphericalangle,u}(z, M_h)}{\left(4 + \frac{1}{2}\right) f_1^u(x)\, D_1^u(z, M_h)} \quad . \tag{50}$$

In the spectator model calculation [110], the nucleon states do not strictly follow the $SU(6)$ symmetry and there is no flavor symmetry for a given distribution. Adopting the same approximation as before, in the spectator model the asymmetries (39) become

$$A_{LU}^{\sin\phi_R \sin\theta}(x, y, z, M_h, Q) = -\frac{W(y)}{A(y)} \frac{M}{Q} \frac{|\boldsymbol{R}|}{M_h} \frac{x \left(4\, e^u(x) - e^d(x)\right) H_{1,sp}^{\sphericalangle,u}(z, M_h)}{\left(4\, f_1^u(x) + f_1^d(x)\right) D_1^u(z, M_h)} \quad , \tag{51}$$

$$A_{UL}^{\sin\phi_R \sin\theta}(x, y, z, M_h, Q) = -\frac{V(y)}{A(y)} \frac{M}{Q} \frac{|\boldsymbol{R}|}{M_h} \frac{x \left(4\, h_L^u(x) - h_L^d(x)\right) H_{1,sp}^{\sphericalangle,u}(z, M_h)}{\left(4\, f_1^u(x) + f_1^d(x)\right) D_1^u(z, M_h)} \quad . \tag{52}$$

The results for the twist-3 PDF $e(x)$, $h_L(x)$, and the unpolarized $f_1(x)$ in the spectator model of Ref. [110] are depicted in Fig. 6 for both the u and d flavor.

In all model results above, the model's scale has been used. This scale turns out to be rather low, $Q_0^2 \sim 0.1$ GeV^2. We neglect the evolution effects on the PDF part of the asymmetries. However, we expect QCD evolution to affect the distributions in pushing them towards lower x values. The missing QCD evolution of the twist-3 PDF is believed to be the largest source of errors in the predictions.

2.6 Predictions for the asymmetries

The dependence of SSA on the variables (z, M_h) are essentially determined by the DiFF, while the Bjorken x-dependence comes mainly from the PDF, shown on Fig. 2, Fig 7, and Fig 8. The latter will strongly depend on the model's features.

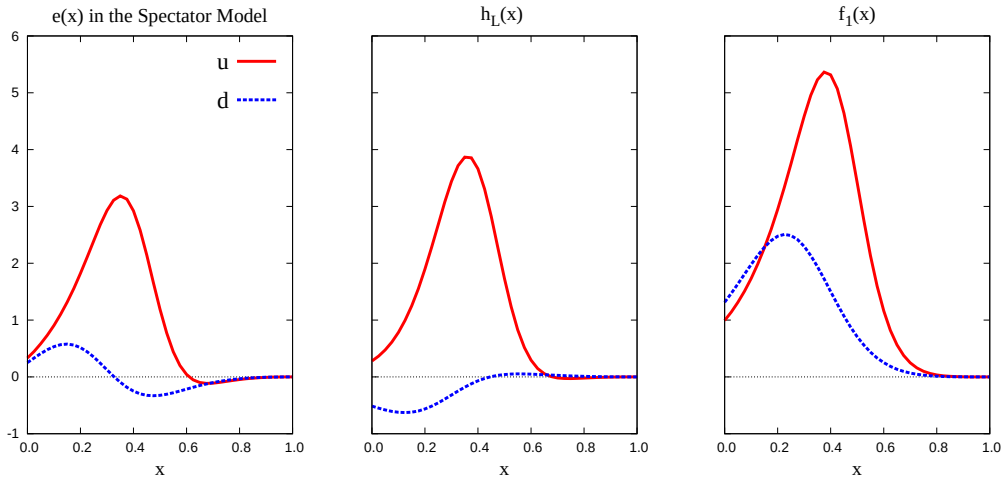

Figure 6: The function $e^q(x)$, $h_L^q(x)$, $f_1^q(x)$, for $q = u$ (solid red line) and $q = d$ (dotted blue line) in the spectator model of Ref. [110].

M_h bin
0.5000 – 0.5329
0.5329 – 0.5981
0.5981 – 0.6810
0.6810 – 0.7504
0.7504 – 0.8133
0.8133 – 1.0000

z bin
0.2250 – 0.3650
0.3650 – 0.4350
0.4350 – 0.4950
0.4950 – 0.5500
0.5500 – 0.6050
0.6050 – 0.6550
0.6550 – 0.7100
0.7100 – 0.7650
0.7650 – 0.8350

x bin	$\langle Q^2 \rangle$ (GeV^2)
0.050 – 0.100	~ 1.3
0.100 – 0.124	~ 1.5
0.124 – 0.148	~ 1.7
0.148 – 0.172	~ 1.9
0.172 – 0.200	~ 2.1
0.200 – 0.232	~ 2.3
0.232 – 0.268	~ 2.5
0.268 – 0.308	~ 3.0
0.308 – 0.376	~ 3.7
0.376 – 0.688	~ 5.6

Table 2: Binning in (z, M_h, x) used in Figs. 7 and 8 as well as the average value for Q^2 for the corresponding x-bin.

The binning chosen for the predictions is given in Table 2.

When presenting the asymmetry binned in z, the numerator and denominator have been separately integrated in z within the bin limits, and over M_h and x from their lowest to highest values in Table 2. The same has been done for the other plots.

A constant value of $Q^2 = 2.5$ GeV^2 is chosen for the projections in z and M_h. On the other hand, since the x variable strongly depends on the scale, we evaluate an average Q^2 for each x-bin. This value is given in the last column of Table 2.

In Figs. 7 and 8, we show the predictions for $A_{LU}^{\sin\phi_R \sin\theta}$ and $A_{UL}^{\sin\phi_R \sin\theta}$ from Eqs. (50 and (52), respectively.

We propose to run with high luminosity, $\sim 10^{35}$ cm^{-2}s^{-1}, yielding an integrated luminosity of ~ 500 fb^{-1}. Measured single and double sub-leading twist asymmetries for pion and kaon pairs in a large range of kinematic variables (x, Q^2, z, M_h and ϕ_R) with unpolarized and

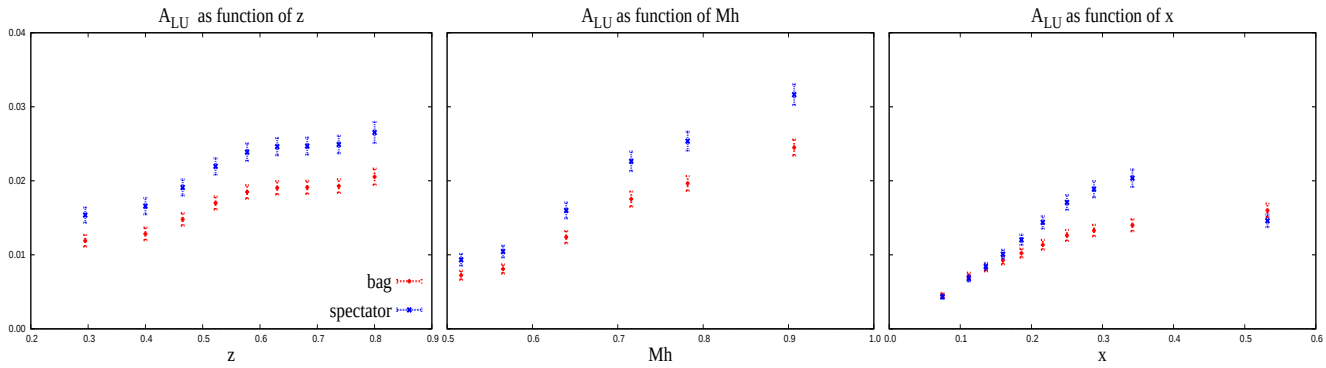

Figure 7: Projections for the asymmetry $A_{LU}^{\sin\phi_R \sin\theta}$ in (z, M_h, x) for $\pi + \pi^-$ pairs. The (z, M_h)-dependence is deduced from the extracted DiFF. The red points are deduced from the x -dependence of PDF in the bag model of Ref. [76], the blue points from the spectator model of Ref. [110].

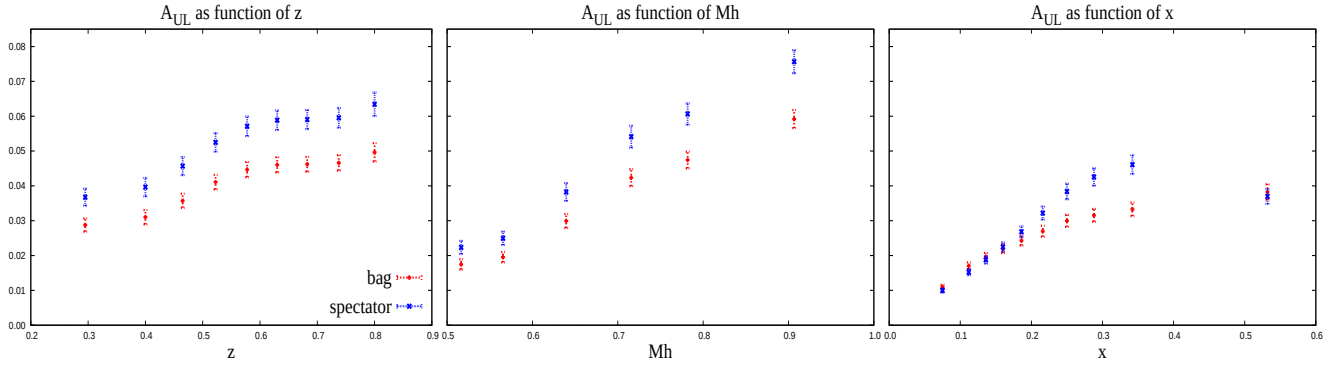

Figure 8: Projections for the asymmetry $A_{UL}^{\sin\phi_R \sin\theta}$ with the same notations as in the previous figure.

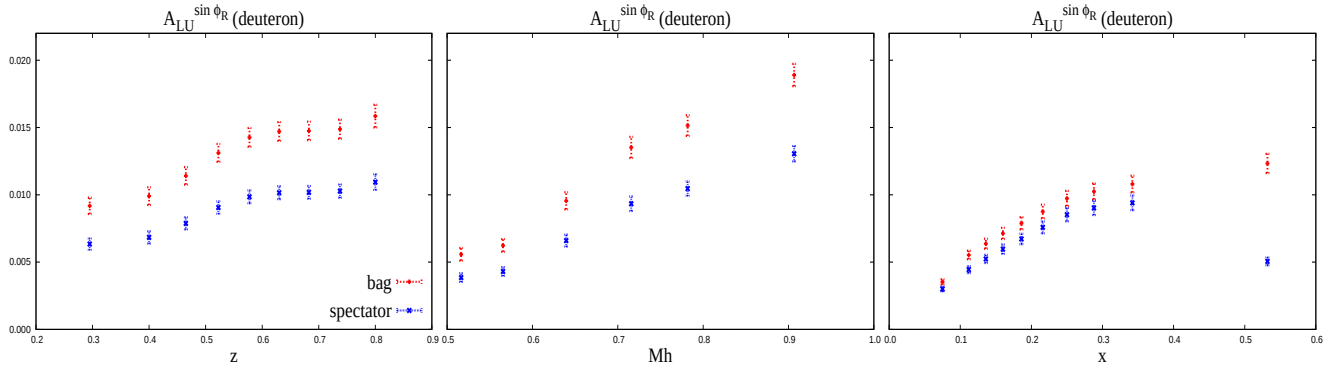

Figure 9: Projections for the asymmetry $A_{LU}^{\sin\phi_R \sin\theta}$ in (z, M_h, x) for $\pi + \pi^-$ pairs for the deuteron target. The (z, M_h)-dependence is deduced from the extracted DiFF. The red points are deduced from the x -dependence of PDF in the bag model of Ref. [76], the blue points from the spectator model of Ref. [110].

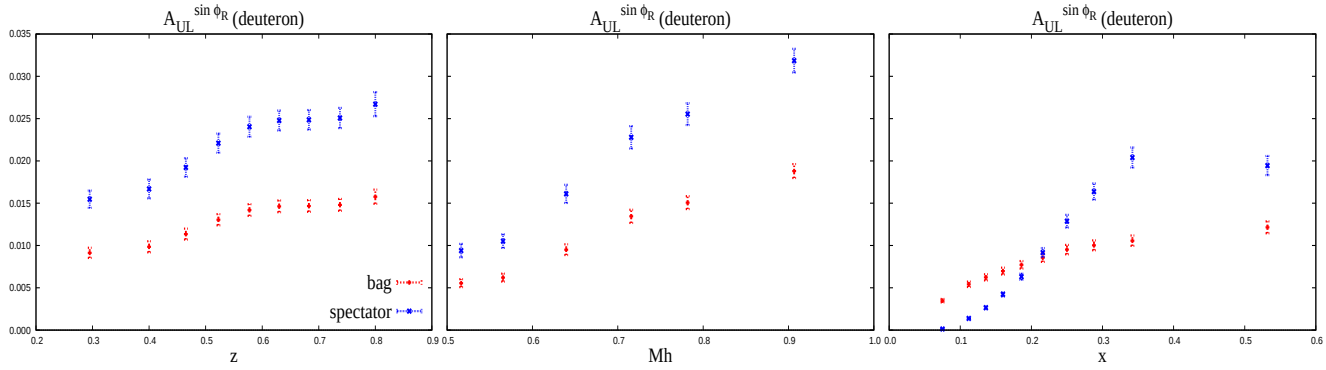

Figure 10: Projections for the asymmetry $A_{UL}^{\sin\phi_R \sin\theta}$ with the same notations as in the previous figure.

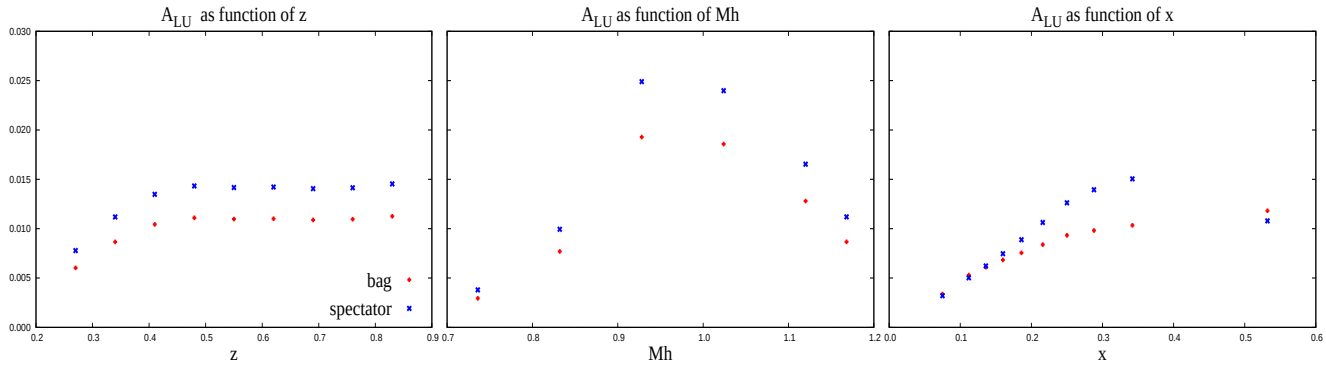

Figure 11: Projections for the asymmetry $A_{LU}^{\sin\phi_R \sin\theta}$ in $(z,\ M_h,\ x)$ for $K+\pi^-$ pairs. The (z, M_h)-dependence is deduced from the simple ansatz of Eq. 42. The red points are deduced from the x -dependence of PDF in the bag model of Ref. [76], the blue points from the spectator model of Ref. [110].

longitudinally polarized targets, combined with similar measurements with single hadrons [131] will provide detailed information on the flavor and polarization dependence of the HT distributions of quarks in the valence region, and in particular, on the x dependence of the HT functions e and h_L.

3 Correlations in hadron production in the current and target fragmentation region

3.1 SIDIS in TFR

As it becomes clear during last decades, to study the three dimensional spin-dependent partonic structure of nucleon the excellent understanding of hadronization process after hard lepton-quark scattering is needed.

The unique feature of CLAS12 detector is the wide coverage of the produced hadrons

phase space: in contrast to old SIDIS experiments, we will have an access not only to current fragmentation region (CFR) but also to target fragmentation region (TFR). These two regions are defined in the virtual photon - target nucleon center of mass frame with z-axis aligned to virtual photon momentum. First one – the CFR – comprise hadrons produced in the forward hemisphere (along the virtual photon) and the TFR – in the backward hemisphere:

$$\ell(l) + N(P_N) \to \ell(l') + h(P) + X \tag{53}$$

with $P_h^3 < 0$.

The QCD description of this process for collinear kinematics includes new nonperturbative objects – the fracture functions first introduced by Trentadue and Veneziano [132]. Recently, this approach was generalized by Anselmino, Barone and Kotzinian [133] to spin and transverse momentum dependent case. The polarized and transverse-momentum dependent fracture functions appear in the expansion of the leading twist projections of hadronic tensor

$$\begin{aligned}
&\mathcal{M}^{[\Gamma]}(x, \mathbf{k}, \zeta, \mathbf{P}_h) \\
&\quad \equiv \frac{1}{4\zeta} \int \frac{\mathrm{d}k^+ \, \mathrm{d}k^-}{(2\pi)^3} \, \delta(k^- - xP^-) \, \mathrm{Tr}\left(\mathcal{M}\,\Gamma\right) \\
&\quad = \frac{1}{4\zeta} \int \frac{\mathrm{d}\xi^+ \, \mathrm{d}^2\xi_\perp}{(2\pi)^6} \, \mathrm{e}^{\mathrm{i}(xP^-\xi^+ - \mathbf{k}\cdot\xi_\perp)} \sum_X \int \frac{\mathrm{d}^3\mathbf{P}_X}{(2\pi)^3 \, 2E_X} \times \\
&\qquad \langle P, S|\bar{\psi}(0)\Gamma|P_h, S_h; X\rangle\langle P_h, S_h; X|\psi(\xi^+, 0, \xi_\perp)|P, S\rangle \,,
\end{aligned} \tag{54}$$

where $\Gamma = \gamma^-, \gamma^-\gamma_5, \mathrm{i}\sigma^{i-}\gamma_5$.

The fracture functions represent the conditional probabilities to find an unpolarized ($\Gamma = \gamma^-$), a longitudinally polarized ($\Gamma = \gamma^-\gamma_5$) or a transversely polarized ($\Gamma = \mathrm{i}\sigma^{i-}\gamma_5$) quark with longitudinal momentum fraction x and transverse momentum $\mathbf{k}$ inside a nucleon fragmenting into a hadron carrying a fraction $\zeta = P_h^-/P^- \simeq E_h/E$ of the nucleon longitudinal momentum and a transverse momentum $\mathbf{P}_h$.

The most general parametrization of the traced fracture matrix for the production of a spinless hadron (54) can be written as:

$$\mathcal{M}^{[\gamma^-]} = \hat{f}_1 + \frac{\mathbf{P}_h \times \mathbf{S}_T}{m_h} \, \hat{f}_{1T}^h + \frac{\mathbf{k} \times \mathbf{S}_T}{m_N} \, \hat{f}_{1T}^\perp + \frac{S_L \, (\mathbf{k} \times \mathbf{P}_h)}{m_N \, m_h} \, \hat{f}_{1L}^{\perp h} \,, \tag{55}$$

$$\mathcal{M}^{[\gamma^-\gamma_5]} = S_L \, \hat{g}_{1L} + \frac{\mathbf{P}_h \cdot \mathbf{S}_T}{m_h} \, \hat{g}_{1T}^h + \frac{\mathbf{k} \cdot \mathbf{S}_T}{m_N} \, \hat{g}_{1T}^\perp + \frac{\mathbf{k} \times \mathbf{P}_h}{m_N \, m_h} \, \hat{g}_1^{\perp h} \,, \tag{56}$$

$$\begin{aligned}
\mathcal{M}^{[\mathrm{i}\,\sigma^{i-}\gamma_5]} &= S_T^i \, \hat{h}_{1T} + \frac{S_L \, P_h^i}{m_h} \, \hat{h}_{1L}^h + \frac{S_L \, k^i}{m_N} \, \hat{h}_{1L}^\perp \\
&\quad + \frac{(\mathbf{P}_h \cdot \mathbf{S}_T) \, P_h^i}{m_h^2} \, \hat{h}_{1T}^{hh} + \frac{(\mathbf{k} \cdot \mathbf{S}_T) \, k^i}{m_N^2} \, \hat{h}_{1T}^{\perp\perp} \\
&\quad + \frac{(\mathbf{k} \cdot \mathbf{S}_T) \, P_h^i - (\mathbf{P}_h \cdot \mathbf{S}_T) \, k^i}{m_N m_h} \, \hat{h}_{1T}^{\perp h} \\
&\quad + \frac{\epsilon_\perp^{ij} P_{h\perp j}}{m_h} \, \hat{h}_1^h + \frac{\epsilon_\perp^{ij} k_{\perp j}}{m_N} \, \hat{h}_1^\perp \,,
\end{aligned} \tag{57}$$

where by the vector product of the two-dimensional vectors we mean the pseudo-scalar quantity $\mathbf{a}_\perp \times \mathbf{b}_\perp = \epsilon_{\perp ij}\, a^i_\perp b^j_\perp = |\mathbf{a}_\perp||\mathbf{b}_\perp| \sin(\phi_b - \phi_a)$. In total there is 16 fracture functions $(\hat{f}, \hat{g}, \hat{h})$ depending on the scalar variables $x, \mathbf{k}^2, \zeta, \mathbf{P}_h^2, \mathbf{k}\cdot\mathbf{P}_h$. Note, that, in contrast with [133], here for fracture functions we use notations corresponding to Amsterdam notations for DFs.

The general LO cross-section expression for SIDIS in the TFR is presented in [133] and give an access only to four quark-transverse-momentum integrated fracture functions.

To have an access to all LO fracture functions one have to "measure" the final quark transverse polarization. The DSIDIS process allows to do that by means of Collins effect for hadron produced in the CFR. Exploiting the SIDIS in TFR and DSIDIS will allow us to check the validity of factorization and deeper understand the hadronization mechanism.

3.2 The Double SIDIS (DSIDIS) process

Let us consider the process in Eq. (1) with first hadron produced in the current fragmentation region (CFR) and second – in the target fragmentation region (TFR) of polarized SIDIS, see Fig. 12.

The LO expression for Spin and Transverse Momentum Dependent (STMD) DSIDIS is given as

$$\frac{d\sigma^{\ell(l,\lambda)+N(P,S)\to\ell(l')+h_1(P_1)+h_2(P_2)+X}}{dx\, dQ^2\, d\phi_S\, dz\, d^2P_{T1}\, d\zeta\, d^2P_{T2}} = \sum_q \mathcal{M}^{h_2}_{q,s/N,S} \otimes \frac{d\sigma^{\ell(l,\lambda)+q(k,s)\to\ell(l')+q(k',s')}}{dQ^2} \otimes D^{h_1}_{q,s'}\,, \quad (58)$$

where $\mathcal{M}^{h_2}_{q,s/N,S}$ STMD fracture functions Eqs. (55–57) , $D^{h_1}_{q,s'}$ are the STMD fragmentation functions to spinless hadron of unpolarized and transversely polarized quarks (see, for example, [52])

$$D^{h_1}_{q,s'}(z,\mathbf{p}) = D_1(z,p^2) + \frac{\mathbf{p}\times\mathbf{s}'}{m_h} H_1(z,p^2), \quad (59)$$

where $\mathbf{p}$ is a transverse momentum of hadron with respect to fragmenting quark momentum.

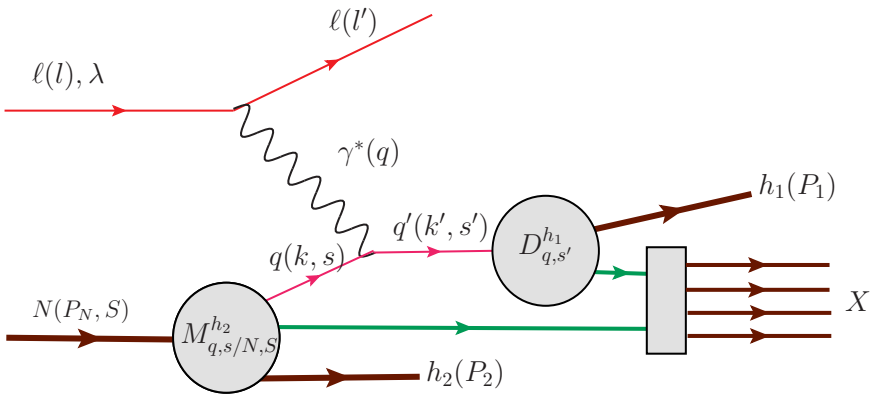

Figure 12: SIDIS description with hadronization function.

3.3 DSIDIS cross section

The cross-section for the DSIDIS of polarized lepton off longitudinally polarized nucleon can be written in the form

$$\frac{d\sigma^{\ell(l,\lambda)+N(P,S)\to\ell(l')+h_1(P_1)+h_2(P_2)+X}}{dx\,dy\,d\phi_S\,dz\,d^2P_{T1}\,d\zeta\,d^2P_{T2}} =$$
$$\frac{\alpha^2\,x}{Q^4 y}\left(1+(1-y)^2\right)\left(\sigma_{UU}+S_L\,\sigma_{UL}+S_T\,\sigma_{UT}+\lambda\,D_{ll}\sigma_{LU}+\lambda\,S_L D_{ll}\,\sigma_{LL}+\lambda\,S_T D_{ll}\,\sigma_{LT}\right)\,, \quad (60)$$

where

$$D_{ll}(y)=\frac{y(2-y)}{1+(1-y)^2}\,. \quad (61)$$

3.3.1 Unintegrated DSIDIS cross section

The terms depending on the longitudinal polarization of initial particles are given by [134]:

$$\begin{aligned}\sigma_{UU} &= F_0^{\hat{M}\cdot D_1} - D_{nn}\left[\frac{P_{T1}^2}{m_1 m_N}\,F_{kp1}^{\hat{h}_1^\perp\cdot H_1}\cos(2\phi_1)\right.\\ &+ \frac{P_{T1}P_{T2}}{m_1 m_2}\,F_{p1}^{\hat{h}_1^h\cdot H_1}\cos(\phi_1+\phi_2)\\ &+ \left.\left(\frac{P_{T2}^2}{m_1 m_N}\,F_{kp2}^{\hat{h}_1^\perp\cdot H_1}+\frac{P_{T2}^2}{m_1 m_2}\,F_{p2}^{\hat{h}_1^h\cdot H_1}\right)\cos(2\phi_2)\right]. \quad (62)\end{aligned}$$

$$\begin{aligned}\sigma_{UL} &= -\frac{P_{T1}P_{T2}}{m_2 m_N}\,F_{k1}^{\hat{M}_L^{\perp h}\cdot D_1}\,\sin(\phi_1-\phi_2)\\ &+ D_{nn}\left[\frac{P_{T1}^2}{m_1 m_N}F_{kp1}^{\hat{h}_{1L}^\perp\cdot H_1}\sin(2\phi_1)\right.\\ &+ \frac{P_{T1}P_{T2}}{m_1 m_2}F_{p1}^{\hat{h}_{1L}^h\cdot H_1}\sin(\phi_1+\phi_2)\\ &+ \left.\left(\frac{P_{T2}^2}{m_1 m_N}F_{kp2}^{\hat{h}_{1L}^\perp\cdot H_1}+\frac{P_{T2}^2}{m_1 m_2}F_{p2}^{\hat{h}_{1L}^h\cdot H_1}\right)\sin(2\phi_2)\right]. \quad (63)\end{aligned}$$

$$\sigma_{LU} = -\frac{P_{T1}P_{T2}}{m_2 m_N}F_{k1}^{\Delta\hat{g}_1^{\perp h}\cdot D_1}\,\sin(\phi_1-\phi_2)\,. \quad (64)$$

$$\sigma_{LL} = F_0^{\Delta\hat{g}_{1L}\cdot D_1}\,, \quad (65)$$

where

$$D_{nn}(y)=\frac{(1-y)}{1+(1-y)^2}\,. \quad (66)$$

The structure functions $F_0^{\Delta\hat{M}_L\cdot D_1}$, $F_{k1}^{\Delta\hat{M}^{\perp h}\cdot D_1}$,...are convolutions of fracture and fragmentation function(see Appendix-B 10).

To compare with observables in single hadron production in target or current fragmentation regions, one can integrate the cross section over the transverse momentum of the second hadron.

3.3.2 DSIDIS cross section integrated over the transverse momentum of the hadron produced in TFR

Consider the DSIDIS with integrated over produced in TFR hadron transverse momentum. In this case the Eq. (60) will contain the hadron transverse momentum integrated fracture functions:

$$\int d^2P_{T2}\,\mathcal{M}^{[\gamma^-]} = \check{f}_1(x,\zeta,\mathbf{k}^2) - \frac{\mathbf{k}\times\mathbf{S}_T}{m_N}\,\check{f}_{1T}^{\perp}(x,\zeta,\mathbf{k}^2)\,, \tag{67}$$

$$\int d^2P_{T2}\,\mathcal{M}^{[\gamma^-\gamma^5]} = S_L\,\check{g}_{1L}(x,\zeta,\mathbf{k}^2) + \frac{\mathbf{k}\cdot\mathbf{S}_T}{m_N}\,\check{g}_{1T}(x,\zeta,\mathbf{k}^2)\,, \tag{68}$$

$$\begin{aligned}\int d^2P_{T2}\,\mathcal{M}^{[\mathrm{i}\,\sigma^{i-}\gamma_5]} &= S_T^i\,\check{h}_1(x,\zeta,\mathbf{k}^2) + \frac{S_L\,k^i}{m_N}\,\check{h}_{1L}^{\perp}(x,\zeta,\mathbf{k}^2)\\ &+\frac{(\mathbf{k}\cdot\mathbf{S}_T)\,k^i - \frac{1}{2}\mathbf{k}^2\,S_T^i}{m_N^2}\,\check{h}_{1T}^{\perp}(x,\zeta,\mathbf{k}^2) + \frac{\epsilon_\perp^{ij}k_j}{m_N}\,\check{h}_1^{\perp}(x,\zeta,\mathbf{k}^2)\,,\end{aligned} \tag{69}$$

where

$$\check{f}_1(x,\zeta,\mathbf{k}^2) = \int \mathrm{d}^2\mathbf{P}_h\,\hat{f}_1\,, \tag{70}$$

$$\check{f}_{1T}^{\perp}(x,\zeta,\mathbf{k}^2) = -\int \mathrm{d}^2\mathbf{P}_h\left(\hat{f}_{1T}^{\perp} + \frac{m_N}{m_h}\,\frac{\mathbf{k}\cdot\mathbf{P}_h}{\mathbf{k}^2}\,\hat{f}_{1T}^{h}\right), \tag{71}$$

$$\check{g}_{1L}(x,\zeta,\mathbf{k}^2) = \int \mathrm{d}^2\mathbf{P}_h\hat{g}_{1L}\,, \tag{72}$$

$$\check{g}_{1T}(x,\zeta,\mathbf{k}^2) = \int \mathrm{d}^2\mathbf{P}_h\left(\hat{g}_{1T}^{\perp} + \frac{m_N}{m_h}\,\frac{\mathbf{k}\cdot\mathbf{P}_h}{\mathbf{k}^2}\,\hat{g}_{1T}^{h}\right), \tag{73}$$

$$\check{h}_{1L}^{\perp}(x,\zeta,\mathbf{k}^2) = \int \mathrm{d}^2\mathbf{P}_h\left(\hat{h}_{1L}^{\perp} + \frac{m_N}{m_h}\,\frac{\mathbf{k}\cdot\mathbf{P}_h}{\mathbf{k}^2}\,\hat{h}_{1L}^{h}\right), \tag{74}$$

$$\check{h}_{1}^{\perp}(x,\zeta,\mathbf{k}^2) = -\int \mathrm{d}^2\mathbf{P}_h\left(\hat{h}_{1}^{\perp} + \frac{m_N}{m_h}\,\frac{\mathbf{k}\cdot\mathbf{P}_h}{\mathbf{k}^2}\,\hat{h}_{1}^{h}\right), \tag{75}$$

$$\check{h}_{1T}^{\perp}(x,\zeta,\mathbf{k}^2) = \int \mathrm{d}^2\mathbf{P}_h\left(\hat{h}_{1T}^{\perp\perp} + \frac{m_N^2}{m_h^2}\frac{2(\mathbf{k}\cdot\mathbf{P}_h)^2 - \mathbf{k}^2\mathbf{P}_h^2}{(\mathbf{k}^2)^2}\,\hat{h}_{1T}^{hh}\right), \tag{76}$$

$$\check{h}_{1}(x,\zeta,\mathbf{k}^2) = \int \mathrm{d}^2\mathbf{P}_h\left(\hat{h}_{1T} + \frac{\mathbf{k}^2}{2m_N^2}\,\hat{h}_{1T}^{\perp\perp} + \frac{\mathbf{P}_{h\perp}^2}{2m_h^2}\,\hat{h}_{1T}^{hh}\right). \tag{77}$$

Note, that the combinations of fracture functions in the r.h.s. enter also in the momentum sum rules derived in [133].

Now, looking at expressions Eqs. (67–69) one immediately can see that they are exactly reproduce the structures entering in decomposition of quark correlators for ordinary TMD

DFs. This means that the LO cross-section expression for considered process will exactly coincide with the LO expression for SIDIS cross section in CFR [52] with the replacement of DFs by corresponding fracture functions in convolutions entering in structure functions

$$\frac{d\sigma^{\ell(l,\lambda)+N(P,S)\to\ell(l')+h_1(P_1)+h_2(P_2)+X}}{dx\,dQ^2\,d\phi_S\,dz\,d^2P_{1T}\,d\zeta} = \frac{\alpha^2 x}{yQ^2}\left(1+(1-y)^2\right)\times$$
$$\times\left[F_{UU}+D_{nn}(y)F_{UU}^{\cos 2\phi_1}\cos(2\phi_1)+S_L D_{nn}(y)F_{UL}^{\sin 2\phi_1}\sin(2\phi_1)+\lambda S_L D_{ll}(y)F_{LL}\right], \quad (78)$$

with

$$F_{UU} = \mathcal{C}\big[\check{f}_1 D_1\big], \quad (79)$$

$$F_{UU}^{\cos 2\phi_1} = \mathcal{C}\left[-\frac{2\left(\hat{\boldsymbol{h}}\cdot\boldsymbol{k}_T\right)\left(\hat{\boldsymbol{h}}\cdot\boldsymbol{p}_T\right)-\boldsymbol{k}_T\cdot\boldsymbol{p}_T}{MM_h}\check{h}_1^{\perp}H_1^{\perp}\right], \quad (80)$$

$$F_{UL}^{\sin 2\phi_1} = \mathcal{C}\left[-\frac{2\left(\hat{\boldsymbol{h}}\cdot\boldsymbol{k}_T\right)\left(\hat{\boldsymbol{h}}\cdot\boldsymbol{p}_T\right)-\boldsymbol{k}_T\cdot\boldsymbol{p}_T}{MM_h}\check{h}_{1L}^{\perp}H_1^{\perp}\right], \quad (81)$$

$$F_{LL} = \mathcal{C}\big[\check{g}_{1L} D_1\big], \quad (82)$$

where the standard notation

$$\mathcal{C}\big[w\,f\,D\big] = x\sum_a e_a^2\int d^2\boldsymbol{k}\,d^2\boldsymbol{p}\,\delta^{(2)}\big(\boldsymbol{k}-\boldsymbol{p}-\boldsymbol{P}_{h\perp}/z\big)\,w(\boldsymbol{k},\boldsymbol{p})\,f^a(x,\zeta,\boldsymbol{k}^2)\,D^a(z,\boldsymbol{p}^2) \quad (83)$$

were used and the unit vector $\hat{\boldsymbol{h}} = \boldsymbol{P}_{h\perp}/|\boldsymbol{P}_{h\perp}|$.

3.3.3 DSIDIS cross section integrated over the transverse momentum of the hadron produced in CFR

For DSIDIS cross section integrated over produced in the CFR hadron transverse momentum the LO expression Eq. (60) will contain the following integrations

$$\int d^2\mathbf{p}\int d^2\mathbf{k}\int d^2\mathbf{P}_1\,\delta^2\left(\mathbf{P}_1-\mathbf{p}1-z\mathbf{k}1\right)\mathcal{M}(x,\zeta,\mathbf{k}^2,\mathbf{P}_2)\mathcal{D}(z,\mathbf{p}_1) =$$
$$\int d^2\mathbf{p}\int d^2\mathbf{k}\,\hat{\mathcal{M}}(x,\zeta,\mathbf{k},\mathbf{P}_2)\mathcal{D}(z,\mathbf{p}_\perp) = M(x,\zeta,\mathbf{P}_2)D_1(z)\,. \quad (84)$$

One can see that in this case we do not access to transversely polarized quark fracture functions and the LO cross-section expression can be obtained as in the case of one hadron production in the TFR [133]:

$$\frac{\mathrm{d}\sigma^{\mathrm{TFR}}}{\mathrm{d}x\,\mathrm{d}y\,\mathrm{d}\zeta\,\mathrm{d}^2\mathbf{P}_h\,\mathrm{d}\phi_S\,\mathrm{d}z} = \frac{2\alpha_{\mathrm{em}}^2}{Q^2 y}\left\{\left(1-y+\frac{y^2}{2}\right)\right.$$
$$\left.\times\sum_a e_a^2\left[\check{f}_1(x,\zeta,\mathbf{P}_h^2)+D_{ll}(y)S_L\,\check{g}_{1L}(x,\zeta,\mathbf{P}_h^2)\right]D_1(z)\,, \quad (85)$$

with

$$\breve{f}_1(x,\zeta,\mathbf{P}_h^2) = \int \mathrm{d}^2\mathbf{k}\, \hat{M}(x,\mathbf{k}^2,\zeta,\mathbf{P}_h^2,\mathbf{k}\cdot\mathbf{P}_h) \tag{86}$$

$$\breve{g}_{1L}(x,\zeta,\mathbf{P}_h^2) = \int \mathrm{d}^2\mathbf{k}\, \hat{g}_{1L}(x,\mathbf{k}^2,\zeta,\mathbf{P}_h^2,\mathbf{k}\cdot\mathbf{P}_h)\,, \tag{87}$$

DSIDIS cross-section LO expressions can be, therefore, studied for three different cases: integrated over TFR hadron transverse momentum, over CFR hadron transverse momentum and unintegrated over transverse momenta. The expressions are rather simple for first two cases, but experimental measurement of azimuthal asymmetries in these cases will be more difficult since azimuthal acceptance corrections will be needed. In the third case the three-dimensional (in azimuths) analysis will allow avoid this problem and will give access to all TMD fracture functions. Measured single and double leading twist asymmetries for pion and kaon pairs in a large range of kinematic variables (x, Q^2, z, $P_{h\perp}$, and ϕ) with unpolarized and longitudinally polarized targets, will thus provide first glimpse to fracture functions.

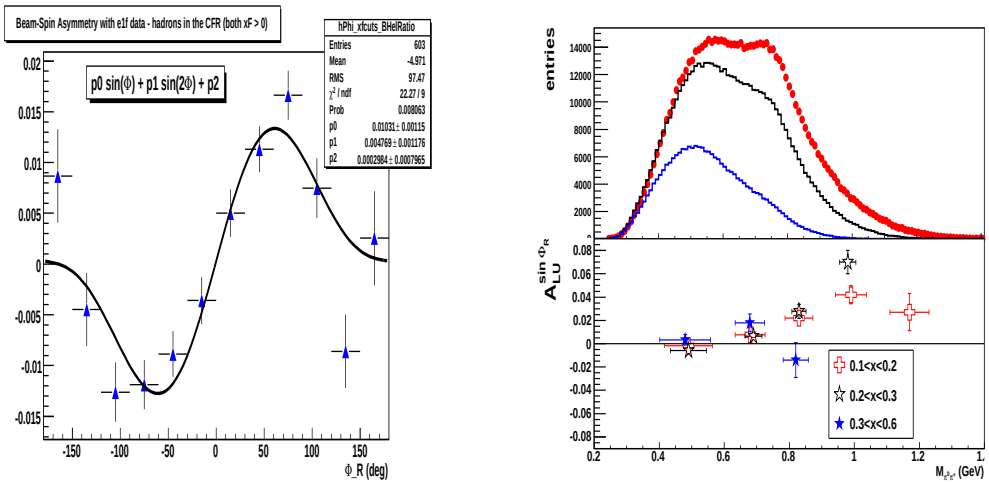

Figure 13: The preliminary beam asymmetry $A_{LU}^{\sin\phi_R}$ for hydrogen target at CLAS 5.7 GeV e1f (left) and e1dvcs (right) experiments.

4 Data on di-hadron production

Measurements of azimuthal moments in dihadron production are available from HERMES and COMPASS. So far the main focus was the leading twist SSA with transverse target. The preliminary data from CLAS at 6 GeV indeed indicate large azimuthal $\sin\phi_R$ moments (see Fig. 13) both for unpolarized and polarized targets involving contributions from corresponding higher twist distribution functions contributing in single hadron and dihadron production.

Dihadron fragmentation functions were studied by Belle Collaborations [14], and used to extract the transversity distribution from SIDIS data. The analysis is in progress for dihadron fragmentation functions with pairs of pions and kaons [135].

Detailed measurements of $A_{LU}^{\sin\phi}$ and $A_{UL}^{\sin\phi}$ asymmetries as a function of relevant kinematical variables in different bins in x, z, Q^2 combined with measurements of single-pion and single-kaon measurements [136, 137, 138] will allow study of the flavor dependence of underlying distribution and fragmentation processes. The CLAS12 with kaon identification provided by the RICH will allow detection of pion-kaon pairs over the full kinematic range, allowing studies of the effect of strange and non-strange sea on the flavor and spin structure of the nucleon.

The goal of our proposed experiment is to gather a data set on hadron pairs produced in SIDIS in the region $0.1 \leq x \leq 0.8$, $0.5 \leq M_h \leq 1.2$, and $0.2 \leq z \leq 0.8$. Global analysis of the data will provide fits to higher twist distribution functions e and h_L.

5 Experimental details

5.1 CLAS12

The proposed experiment will run in two stages. In the first stage running conditions will be similar to an already approved CLAS12 proposal for semi-inclusive DIS studies with CLAS12 [136, 137] with unpolarized proton and deuteron targets. In the second stage running conditions will be similar to an already approved CLAS12 proposal for semi-inclusive DIS studies with CLAS12 [139, 138] for longitudinally polarized proton and deuteron targets.

We will use the upgraded CLAS12 spectrometer with the low threshold Cherenkov counter replaced by the RICH detectors. We will run at the standard magnetic field in both stages, as close to identical acceptances for both experiments will simplify the global data analysis. The central tracker will also be used for coincident detection of protons, pions and kaons both in target and current fragmentation regions. The solenoid for the central tracker is also used simultaneously to provide the magnetic field for the polarized target.

5.2 CLAS12 Particle Identification

In the baseline design of CLAS12, particle identification (PID) in the forward detector is obtained by using the high threshold Cerenkov counter (HTCC), the low threshold Cerenkov counter (LTCC) and the Time-of-flight scintillator arrays (TOF) (see Fig. 14). In the $\sim 2.5-5\ GeV/c$ momentum region, the π/K separation relies only on the LTCC performance. Moreover, in the $4.7-8\ GeV/c$ momentum region it is not possible to separate protons from kaons. In general, this PID system matches the requirements of the physics program at 12 GeV. However there are some physics reactions of high interest, such as the one covered by this proposal, that cannot be accessed without a better PID, especially for charged kaon detection. At 12 GeV for semi-inclusive processes, the K/π ratio is of the order of $10-15\%$ (see Fig. 15) thus the required rejection factor for pions is around $1:1000$ (corresponding to 4.7σ pion-kaon separation) while with the present configuration, assuming a pion detection inefficiency for the LTCC of 10%, the π/K contamination is $1:1$. A RICH detector, to be installed in place of the low threshold Cerenkov counter, will significantly improve the CLAS12 particle identification overcoming the above limitations without having any impact on the baseline design of CLAS12.

5.3 CLAS12 RICH detector

To fit the CLAS12 geometry, the RICH should have a projective geometry with six sectors matching the torus bores and covering scattering angles from 3° to 30° (see Fig. 16). Being downstream to the torus magnet at more than 5 m from the interaction point, the RICH has to cover a large surface, each sector having an area of the order of 4 m^2 in the front and 8 m^2 in the back. The RICH depth cannot exceed 1 m, being the detector constrained between existing equipments; the proposed solution is based on the concept of the proximity focusing RICH, with mirrors mainly devoted to reduce the photon detector area. In the momentum range of interest an aerogel RICH represents the best solution for the identification of $\pi/K/p$

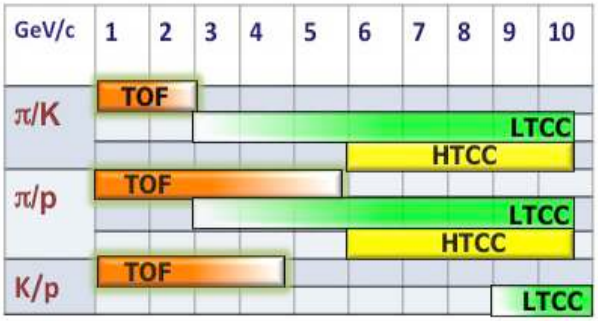

Figure 14: Hadron particle identification in CLAS12.

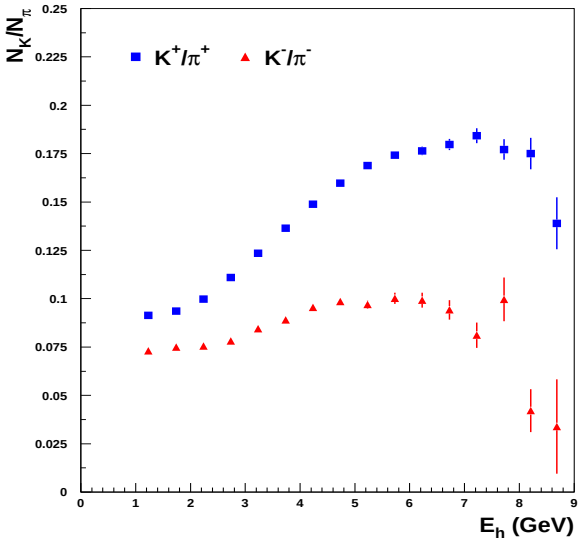

Figure 15: Semi-Inclusive kaon versus pion yield ratio.

as shown in Fig. 17. This implies detecting Cherenkov light in the visible wavelength range and using photomultipliers (PMTs) as photon detectors. On going Monte Carlo studies (see next section) show that a pion-kaon separation greater then 4 σ at 8 GeV/c momentum can be achieved if the detector pad size is less than 1x1 cm^2, thus the use of Multi-Anode PMTs is mandatory.

The use of aerogel as radiator and the detection of light in the visible wavelength range is an expensive solution. Work is in progress to limit the area of the photon detector to about $1m^2$ per sector. The study of the spatial distributions of the Cherenkov photons impact point at the detection surface shows that high-momentum particles concentrate in a limited forward region close to the beam line (see Fig. 18).

The approach is, thus, to instrument a limited area around the beam line to have direct detection in the forward region at high momenta, while at large angles and lower momenta

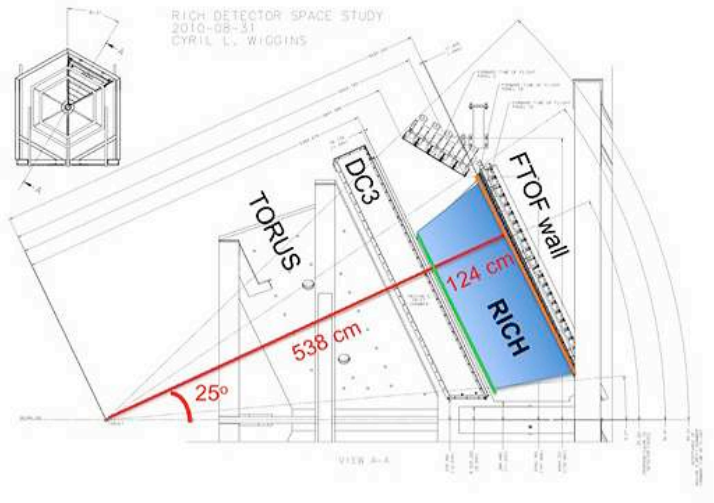

Figure 16: RICH detector space and position in the CLAS12 spectrometer.

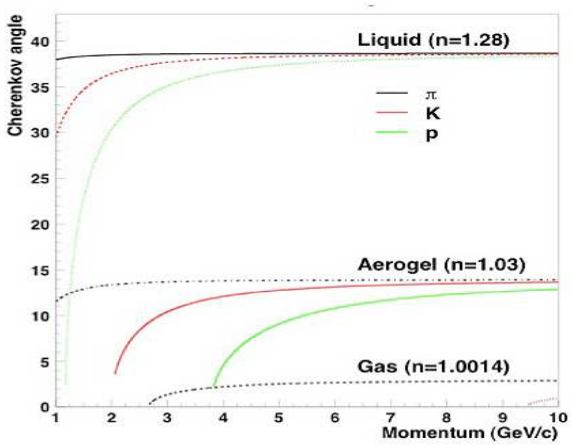

Figure 17: Cherenkov angle versus particle momenta for π, k, p and different radiators.

a system of focusing mirrors catches the light and reflect it toward the photon detector. A drawing of the proposed solution is illustrated in Fig. 19 where the main components of the systems are shown: the planar mirror (positioned before the aerogel), the aerogel, the proximity gap, the PMTs plane covering the angular region between 3° and 14°, and the elliptical mirror which reflects the light produced by the particles emitted at angles larger than 14° towards the planar mirror.

5.3.1 Preliminary Monte Carlo results

Preliminary Monte Carlo studies based on GEANT4 with a realistic geometry of the CLAS12 detector and events generated with Pythia have been performed with the aim to optimize all the componenent of the detector. The dimensions of the radiator thickness and the gap

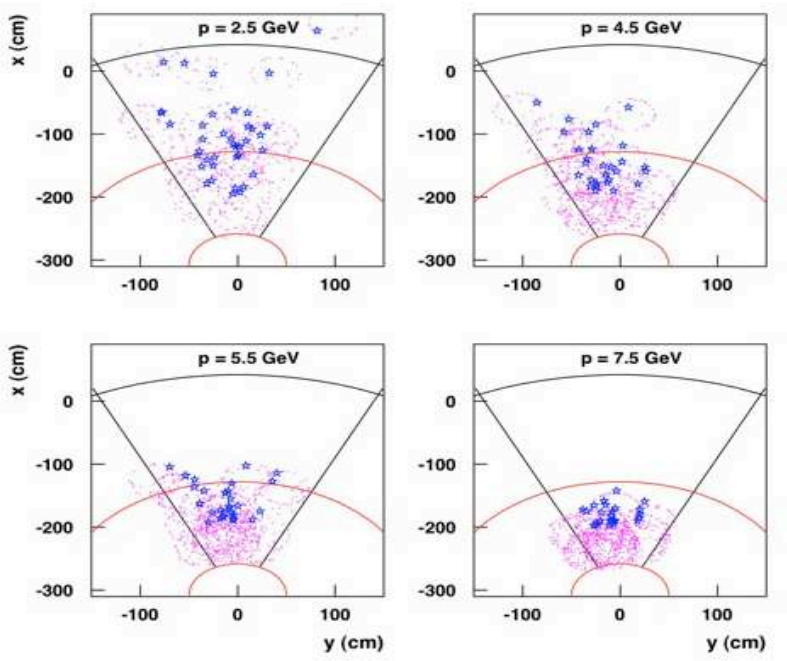

Figure 18: Spatial distributions of the particle impact point at the RICH entrance (stars) and gamma impact point at the detector surface (dots) for few overlapped events. The plots distinguish among particle of increasing average momentum, from 2.5 GeV/c up to 7.5 GeV/c, from top to bottom and left to right. High-momentum particles concentrate in a limited forward region close to the beam line, arbitrarely delimited by the two dashed lines just for an illustration purpose.

length as well as the pad/pixel size of the photon detector have been varied in order to find the optimal combination which gives the smallest reconstruction error in the Cerenkov angle and the highest number of photoelectrons. An average number of 10 and 5 photoelectrons has been obtained for the direct and reflected light collection, respectively. An example of simulated events in the proposed RICH geometry is shown in Fig. 20 where Cherenkov light direct detected and detected after the elliptical mirror reflection is clearly visible.

In order to have a precise information about the RICH performances in terms of pion/kaon separation a pattern recognition algorithm based on the event-wise Direct Ray Tracing (DRT) technique has been implemented; DRT combines the track(s) information with all feasible hypotheses on the tracking particle(s) and realistically estimates, for each hypothesis, the produced photon hits patters, which are combined to the simulated/measured one by means of a likelihood function. The most probable particle(s) hypothesis is assumed as the true one. The results obtained using the RICH configuration shown in Fig. 19 with aerogel of increasing thickness from 2 to 6 cm, a gap length of ~ 100 cm and a pad size of 0.6 cm and for particle momenta in the range 7-9 GeV/c is shown in Fig. 21. In the figure the likelihood for the different particles hypothesis is shown. As it can be seen the contamination is widely smaller than 1%. For istance, the probability that a pion is misidentified as a kaon is 0.18% which corresponds to approximatively a 4-5 σ pion/kaon separation.

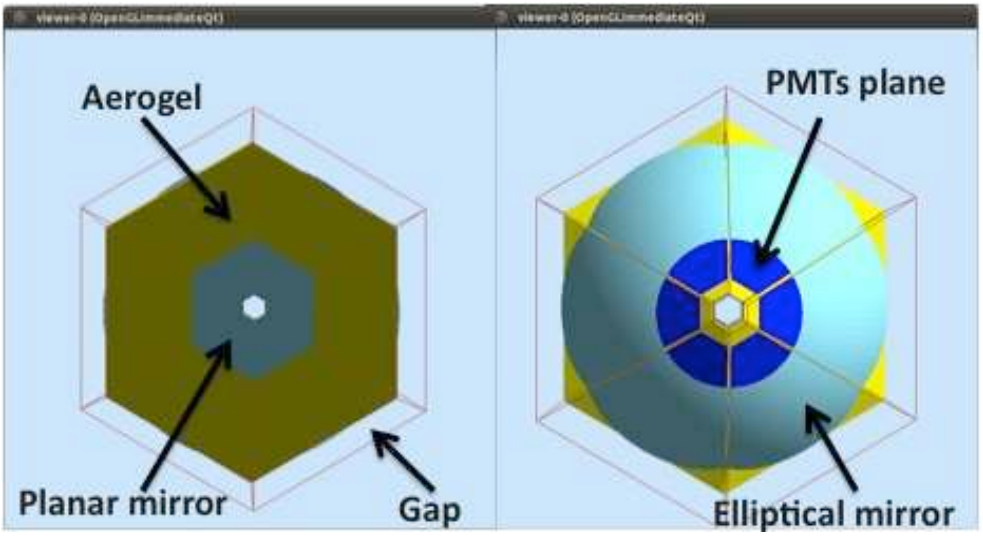

Figure 19: Drawing of the proposed proximity focusing RICH with focusing mirrors.

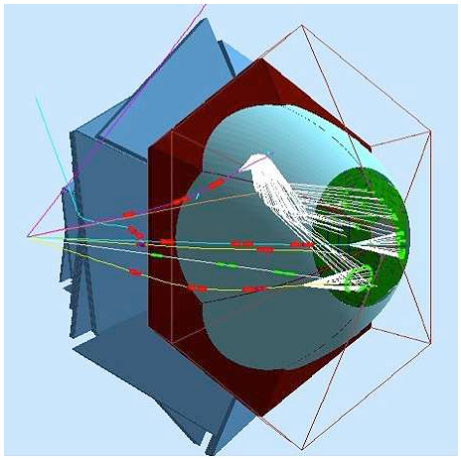

Figure 20: Exemple of events simulated with GEANT4

The preliminary results of the ongoing Monte Carlo analysis are ecouraging about the performances of the proposed RICH; several potential improvements have been already identified and are under detailed investigation. Also test in realistic conditions of the proposed solution with a small prototype is underway.

5.4 The unpolarized target

We propose to use a collinear, dual-cell target containing deuterium (for the primary measurements of multiplicities and the extraction of the shape of strange PDF) and hydrogen (for fragmentation function measurements on proton). Measurements of cross section differences for unpolarized proton and deuteron targets will benefit from similar systematics due

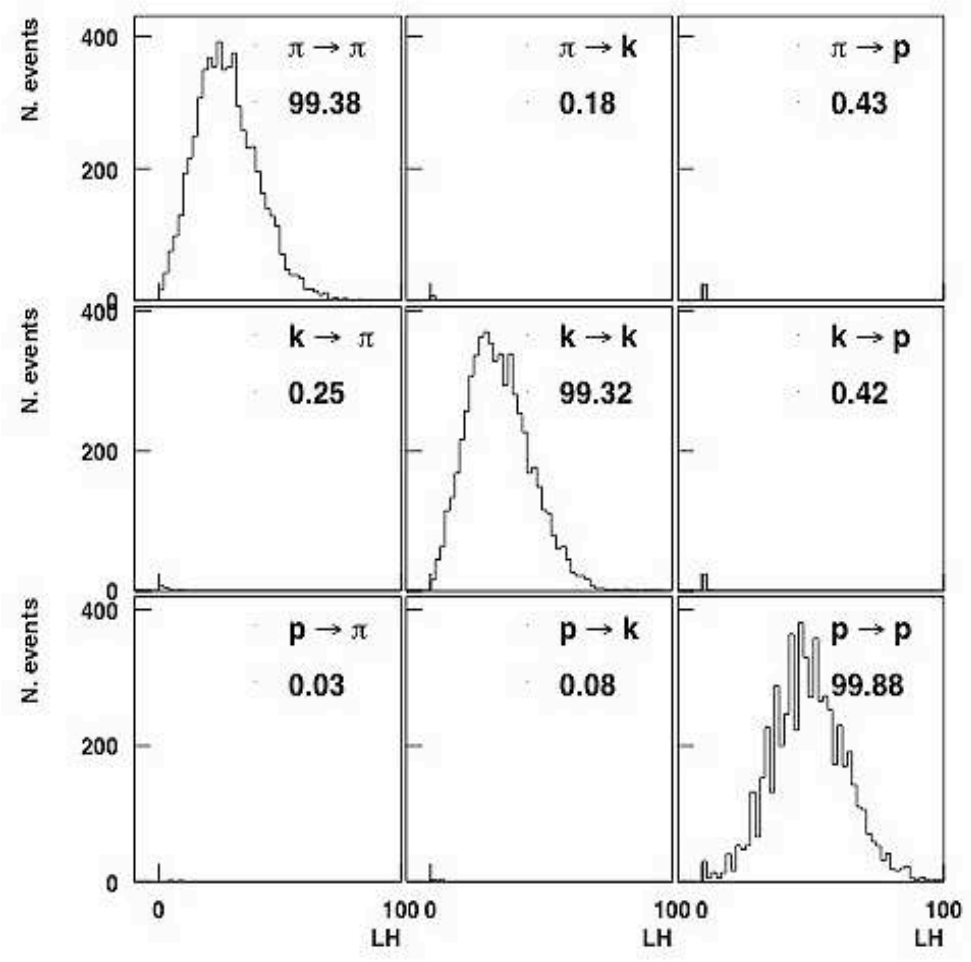

Figure 21: Likelihood distribution for the different particles hypothesis.

to simultaneous measurements, allowing to do a flavor dependence analysis for the higher twist function e. The dual-cell target will be similar in design to the one used for the CLAS measurements of G_M^n [140] during the E5 running period. A conceptual drawing of the target is shown in Figure 22. Each of the cells containing liquid will be 2 cm in length with a 1.0 cm gap in between. The length of the cells is designed to fit within the current design of the CLAS12 silicon vertex tracker. To measure effects due to different target positions, we will collect data with the targets in opposite cells from the default configuration.

5.5 The polarized target

The target configuration will be the same as for already approved proposals using the polarized target [139, 131, 137]. It will be polarized via the method of Dynamic Nuclear Polarization (DNP) which is a well established technique that has been used extensively in nuclear and particle physics experiments, including the ones performed in Hall B of Jefferson Lab. Dynamically polarized target systems consist of a hydrogenated (polarized protons)

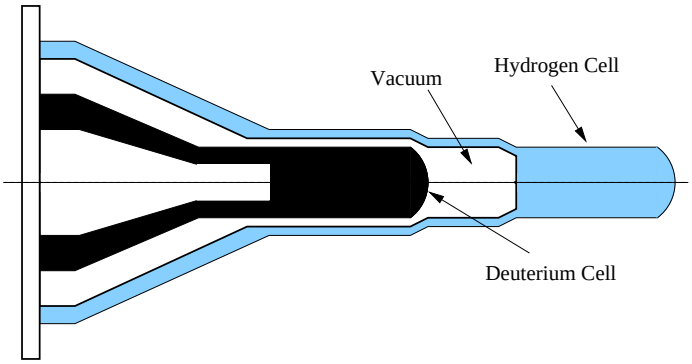

Figure 22: The conceptual design of the dual-target cell [141].

or deuterated (polarized neutrons) compound containing paramagnetic centers, such as unpaired electrons, placed in a high magnetic field and cooled to low temperatures, with a B/T ratio of the order of 5 Tesla/Kelvin. In these conditions, the free electron spins can approach polarization of 100%. The high polarization of unpaired electrons is then transferred dynamically to the nucleons by irradiating the target material at frequency near that of electron spin resonance. This technique typically achieves a proton polarization of 80-90%, and a deuteron polarization of 30-40%. The nucleons in the target will be polarized either parallel or anti-parallel to the electron beam direction.

The main systems required to realize DNP are the superconducting magnet to provide a strong (5 T) field, a ^{4}He evaporation refrigerator to maintain the target material at 1 K, a target insert, which will house the target material and some additional instrumentation, a microwave system to transfer the polarization to the nucleon spins, and a Nuclear Magnetic Resonance (NMR) system to determine the state of polarization.

In CLAS12 the polarizing magnetic field will be provided by the superconducting solenoid of the central detector. Ammonia and deuterated ammonia will be used as target material with the electron beam and CLAS12. In order to determine the dilution factor (fraction of events originating from unpolarized target materials) for each process with sufficiently high accuracy, about 20% of the running time will be devoted to measurements with carbon, nitrogen, and helium. To determine the proton to deuteron and deuteron to carbon cross section ratios, we will need a few days of running with the same magnetic fields and target position as the present experiment, but with gas or liquid hydrogen and deuterium targets. We anticipate that this can be scheduled in conjunction with other planned experiments with CLAS12.

For measurements on polarized deuterium, we may choose to use ^{6}LiD or HD as the target material, rather than ND_3. Both targets provide a very substantially better dilution factor, and therefore substantially smaller statistical and systematic errors, for a given target polarization and luminosity. In the case of ^{6}LiD, the good dilution factor arises through the assumption that ^{6}LiD can be regarded to first approximation as an unpolarized alpha particle bound with a polarized deuteron. Planned test with frozen spin HD target will show if this target can withstand the heat load of a sufficiently high beam current to make this target material competitive with ND_3 or ^{6}LiD. If so, the very good dilution factor (over 50%) and

lack of nuclear corrections from polarized nitrogen or lithium will make this the target of choice. The target polarization will be monitored during the run via the NMR system, in the field of solenoid magnet. The calibration of the proton NMR can be done by measurements of polarization in thermal equilibrium, taken with the polarizing magnet.

The experiment will run with a beam of about 10 nA on a 3 cm long ammonia target, resulting in a luminosity of $10^{35}/\mathrm{cm}^2\mathrm{s}$. The beam will be rastered over the diameter of the polarized target (about 3 cm) to minimize the dose density (we will need at most one anneal every other day under these conditions).

6 The data set and analysis

The expected kinematical coverage in the DIS region from the proposed experiment with 11 GeV beam and CLAS12 is shown in Fig.23. This will constitute a substantial increase over the existing Jefferson Lab data in both x and Q^2 (maximum Q^2 of 5 GeV^2 and x between 0.2 and 0.6), while the precision of the expected data in the valence region will be far superior to existing DIS experiments from other labs.

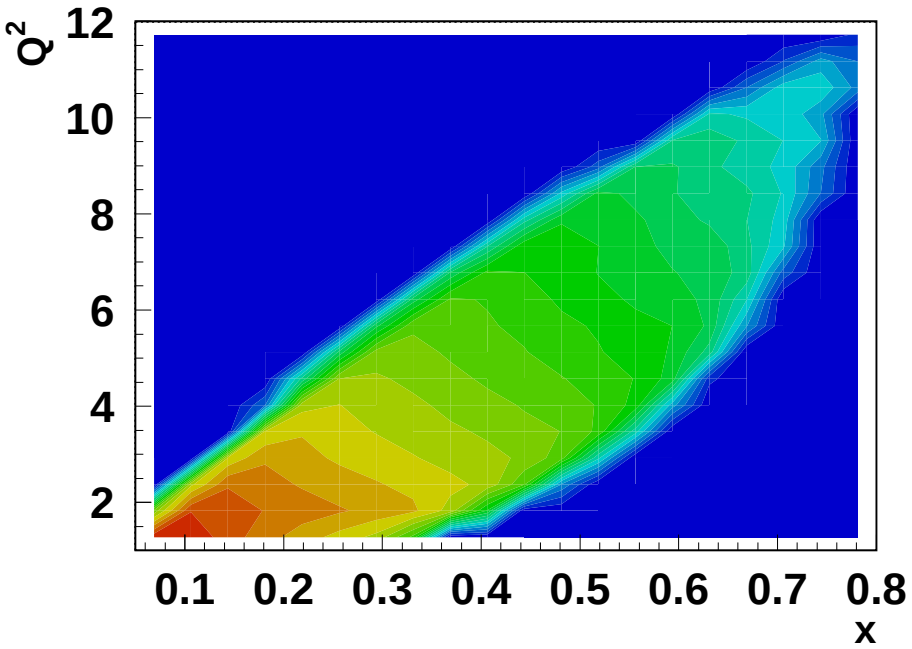

Figure 23: Kinematical coverage in the SIDIS region of the proposed experiment for $ehhX$ events.

Realistic MC simulations are crucial for separation of different contributions to $\cos\phi$ and $\cos 2\phi$ azimuthal moments arising from higher twists, both kinematical [142] and dynamical

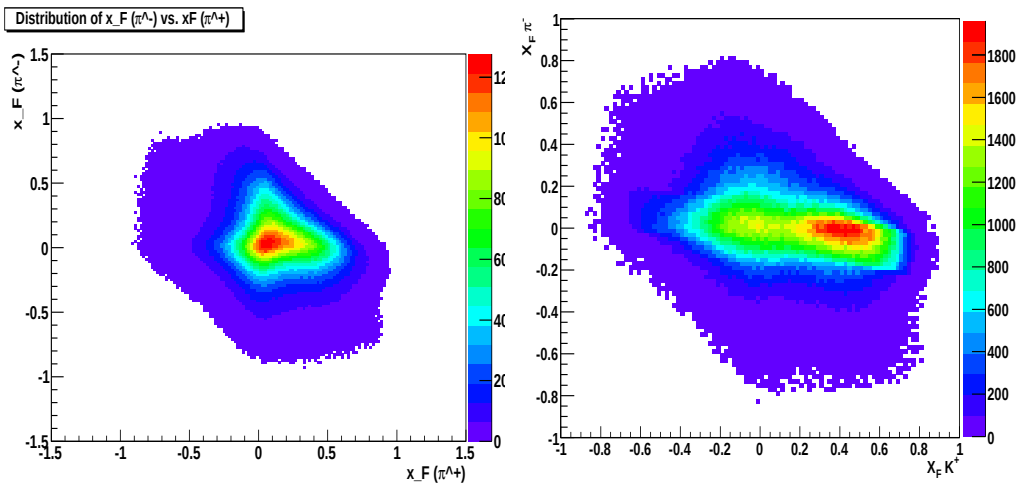

Figure 24: Distribution over x_F for pion-pion and pion-kaon pairs from FASTMC

[143, 144, 145, 146], radiative corrections [147, 148] and in particular from the detector acceptance. The CLAS12 FAST-MC program was used to simulate the physics events and study the extraction of azimuthal moments and acceptance corrections. Large acceptance of CLAS12 allows detection of final state hadrons produced both in target and current fragmentation regions. The 2D x_F-distributions are shown on Fig. 24. Selecting different kinematical regions one can measure azimuthal asymmetries in those regions and extract underlying non-perturbative functions.

6.1 The unpolarized data set and analysis

One of the main goals of the experiment will be to extract the $\sin\phi$ ($A_{LU}^{\sin\phi}$) moments as functions of Q^2, x, P_T,z, and M_{hh}. To estimate the accuracy we will be able to achieve in the measurement of response functions, we used studies with hadron pairs processed through CLAS12 *FastMC* to obtain the simulated detector "data". The "data" were then acceptance corrected to obtain the differential cross sections. Beam spin asymmetries are simulated by extracting $(N^+ - N^-)/(N^+ + N^-)$ for each bin where $N^{\pm}$ are the number of events from $\pm$ electron helicity. These asymmetries were then fit by a function $Asin\phi/(1+Bcos2\phi+Ccos\phi)$, where A is related to the $A_{LU}^{\sin\phi_R}$ moment. It was demonstrated that the $A^{\sin\phi_R}$ moments can be extracted over a very large kinematic range.

6.1.1 The data set and analysis

In projected results we assume a beam polarization of 0.85, which has been routinely achieved in recent experiments running at Jefferson Lab. The beam helicity will be flipped in a pseudo-random pattern every 33 ms. We will use the standard Hall B beam devices to monitor and stabilize the beam intensity and position. In particular, we will reduce any helicity-correlated beam asymmetries to less than 10^{-3}.

The first-level trigger will consist of a coincidence between the high-threshold Cerenkov counter and a signal above threshold (corresponding to at least 1 GeV deposited) in the

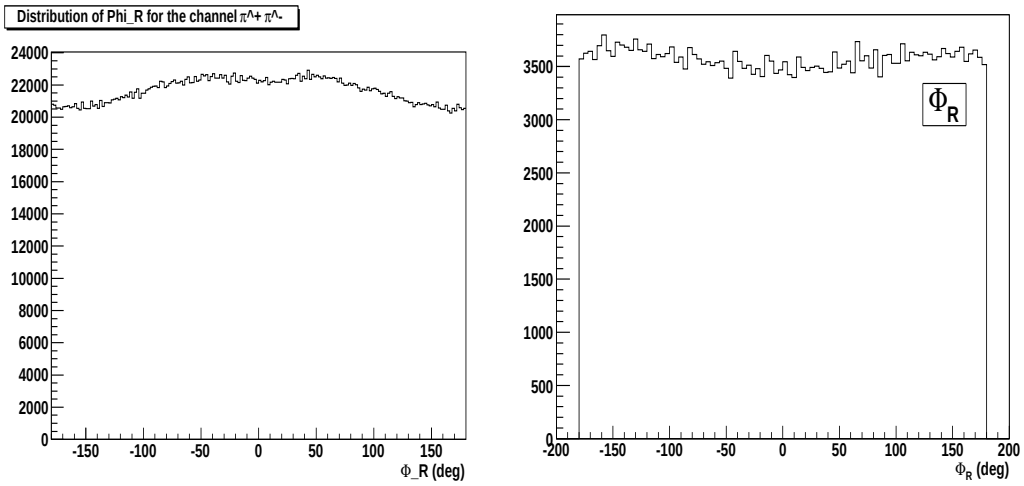

Figure 25: Distribution over ϕ_R for pion-pion and pion-kaon pairs from FASTMC

electromagnetic calorimeter in the same sector. This trigger will be highly specific for high-energy electrons, with little contamination from pions and other particles. In the case of too high background, we can also implement a level 2 trigger, which requires a electron candidate track in the drift chambers of the same sector as the level 1 trigger. This has already been developed for the present CLAS. The total event rate in the DIS region for this experiment is expected to be around 2000 Hz above $Q^2 = 1$ GeV^2. Estimated total maximal trigger rates that DAQ can handle are around 20 kHz. A data acquisition rate of 10 kHz has already been achieved with today's technology for the present CLAS DAQ. So that the required data acquisition rate for this experiment is a rather modest.

The data will consist of the number of counts for beam electron or target proton helicity parallel (N^+) and anti-parallel (N^-) states, each normalized to the dead-time corrected integrated beam charge. We will subtract from these rates the backgrounds from misidentified kaons/pions (which can be obtained from fits to the distribution of photo-electrons in the high-threshold Cerenkov counter and the measured ratio of visible energy deposited in the electromagnetic calorimeter to the measured momentum) and from electrons coming from pair-symmetric decays (e.g., $\pi^0 \to e^+e^-$ or $\pi^0 \to \gamma e^+e^-$ as well as $\gamma \to e^+e^-$ conversions). From the corrected counts, we will form the ratio $A^{raw} = (N^+ - N^-)/(N^+ + N^-)$. This ratio has to be divided by the beam or target polarization and the additional dilution factor for the polarized target case (the fraction of counts coming from the polarized nuclei in the target to the total).

For polarized target configuration, following the procedure developed for the single-hadron case [138], the dilution factor can be calculated from a detailed model of the target content. The only ingredient needed is the packing fraction (the fraction of the cell volume occupied by the ammonia beads), which can be extracted by comparing the rate from ammonia to that from an auxiliary carbon target. Additional measurements on empty and liquid-helium only targets will also be needed. Past experience with the EG1 experiment in Hall B has shown that a typical error of 3% on the dilution factor can be achieved [149]. An additional correction for the small polarization in ^{15}N and contamination by ^{14}N and, in the case of the deuterated ammonia, H, will be applied as well.

6.1.2 Single-spin azimuthal asymmetries

The beam (P_B) and target (P_T) polarization will be independently measured using Möller scattering and NMR, respectively. The target polarization, however, can be extracted from the product of $P_B * P_T$ with higher precision directly from our data, by measuring the asymmetry of elastic (quasi-elastic) scattering $\vec{p}(\vec{e}, e'p)$ ($\vec{d}(\vec{e}, e'p)$) from our NH_3 (ND_3) targets, respectively. We did a full simulation of this method, including radiative effects, CLAS12 acceptance, and expected beam parameters. We find that the uncertainty on P_T for the proton will be about 3% and on the deuteron about 5%.

Measurements of average moments $\langle W(\Phi)\rangle_{LU/UL} = \int \sigma_{LU/UL}(\Phi) W(\Phi) d\Phi / \int \sigma(\Phi) \sin^2\phi d\Phi$ ($W(\phi) = \sin\Phi, \sin 2\Phi$) of the cross section $\sigma^{W(\Phi)}_{LU/UL}$ will single out corresponding terms in the cross section. Thus the $\sin\Phi$ SSA of the cross section for longitudinally polarized target and unpolarized beam is defined as:

$$A^{\sin\Phi}_{LU/UL} = \frac{\langle \sin\Phi\rangle_{UL/LU}}{\langle \sin^2\Phi\rangle_{UU}} = \frac{1}{P^{\pm}N^{\pm}} \frac{\sum_{i=1}^{N^{\pm}} \sin\Phi_i}{\sum_{i=1}^{N^{\pm}} \sin^2\Phi_i},$$

where $P^{\pm}$ and $N^{\pm}$ are the polarization and number of events for $\pm$ helicity state, respectively, and Φ will be Φ_R, $\phi_1 - \phi_2$, $\phi_1 + \phi_2$,$2\phi_1$,..., depending on the observable. For spin-dependent moments this is equivalent to the corresponding spin asymmetries $A^W_{UL/LU}$. The final asymmetry is defined by the weighted average over two independent measurements for both helicity states or by fitting with corresponding azimuthal dependences ($\sin\Phi, \cos\Phi$) the spin asymmetries binned in the azimuthal angle and $\sin\theta$.

The single-spin asymmetries in di-hadron SIDIS for charged and neutral hadron pairs are sensitive to HT parton distributions through the different flavor sensitivities tagged by the hadron charge. The systematic errors largely cancel in the ratios of PDFs allowing for measurements with statistical and systematic precision of $\sim$3% in bins in x, z and M_{hh}.

7 Expected results

7.1 Simulation

The CLAS12 FAST-MC program was used to simulate the physics events and study the extraction of azimuthal moments and acceptance corrections. The expected number of counts and corresponding statistical errors in the following sections are based on a full simulation of inclusive and semi-inclusive inelastic scattering with the CLAS12 acceptance folded in. Events were generated with the clas12DIS generator [150]. This generator is basically an implementation of the LUND Monte Carlo package called PEPSI (Polarized Electron-Proton Scattering Interactions) [151]. It is based on polarized and unpolarized parton distribution functions and the LUND string model for hadronization (both in target and current fragmentation region), and has been tested successfully against several low-Q^2 experiments with 5.7 GeV beam at Jefferson Lab.

A fast Monte Carlo simulation program has been used to define the acceptance and resolution of the CLAS12 detector with all of the standard (base) equipment in place. The kaons were assumed identified 100% in sectors covered by CLAS12-RICH, and also at energies above 5 GeV, where the pions start to fire the High Threshold Cherekov Counter (HTCC). The events generated by clas12DIS are used as input and all particles are followed through all detector elements.

The resolution of the detector is simulated by a simple smearing function which modifies a particle's track by a random amount in momentum and angles according to a Gaussian distribution of the appropriate width. The amount of smearing follows the design specifications of the CLAS12 detector. The resolution in x varies between $0.01 < \sigma_x < 0.035$ and is therefore finer than our planned x bin size of 0.05 in all cases.

A full Monte Carlo simulation (GEANT-based) of CLAS12 with all resolution effects will be used to determine the effective mean x (and Q^2) for each x-bin we will use to bin our data so we can accurately extract the x-dependence of the measured asymmetries.

7.2 Statistical and systematic errors

The proposed single-spin asymmetry measurement is rather insensitive to uncertainties in acceptances and charge normalization. A cut on the missing mass of the dihadron pairs will be used to suppress contamination from exclusive production. The missing mass distributions for different hadron pair combinations are shown in Fig. 26. Various kinematic distributions for two hadron production are shown on Figs.25-32. A cut on the $x_F < 0$ and $x_F > 0$, (x_F is the fraction of the longitudinal momentum in the center of mass frame) was used to separate particles in target fragmentation region (TFR) and the current fragmentation region (CFR), respectively. The overall statistics of pion-kaons pairs is an order of magnitude less than for pion-pion pairs, with most of the relevant sources of systematic errors being the same.

Other sources of systematic errors include the beam and target polarizations, dilution factor the longitudinal to transverse photo absorption cross section ratio, $R(x, Q^2)$. The main sources of systematic errors in measurements of single and double spin asymmetries are listed in the Table 3. These errors are all scale errors, so they are proportional to the size of the measured asymmetry. The total uncertainty is expected to be less than 10% of

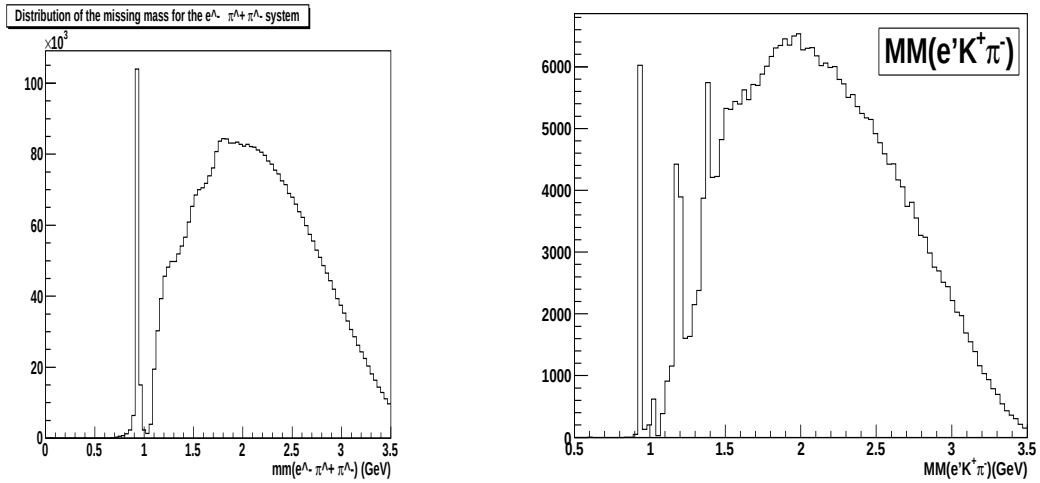

Figure 26: Missing mass distributions for kaons and pion pairs from PEPSI MC for $ehhX$ events.

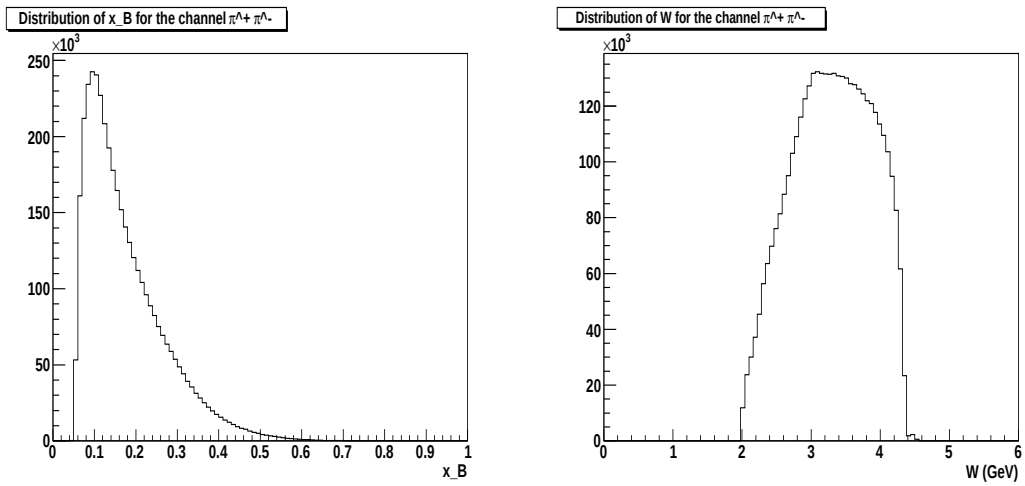

Figure 27: x and W-distribution of pion pairs.

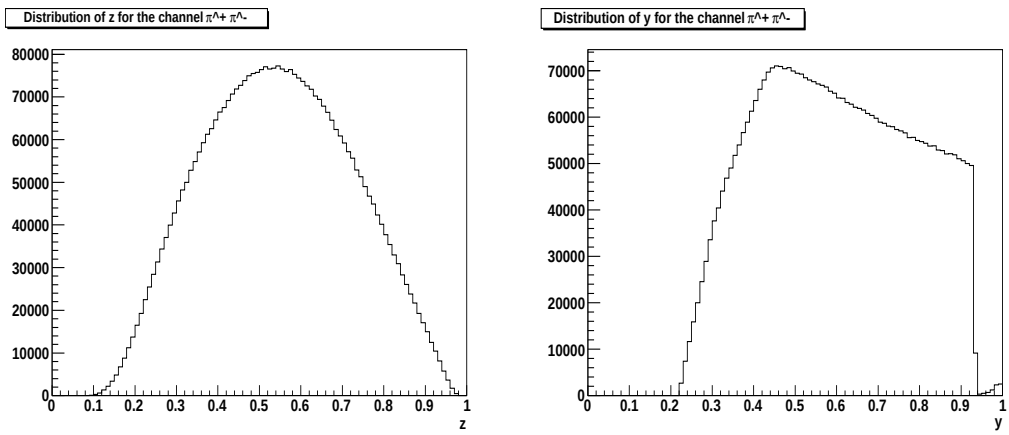

Figure 28: z and y-distributions of pion pairs.

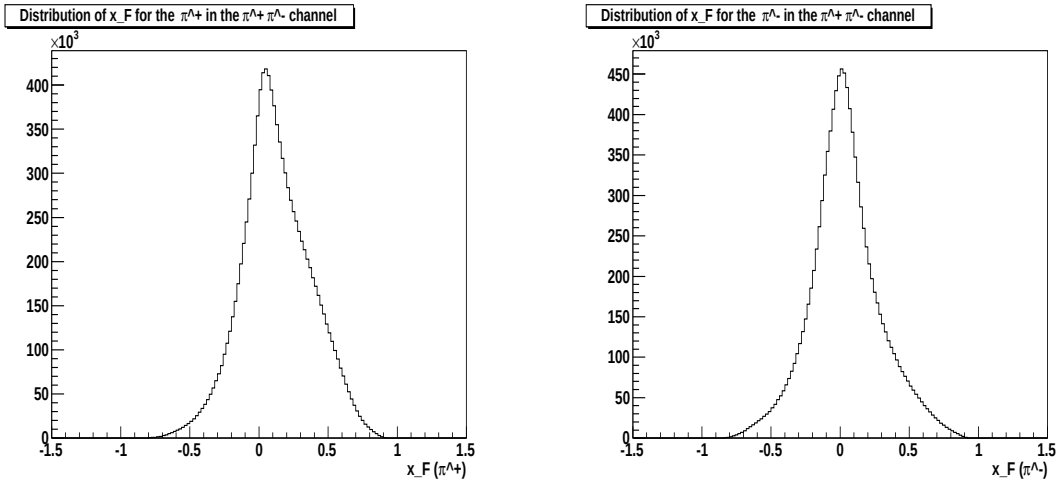

Figure 29: x_F-distributions of π^+ (left) and π^- (right) of pion pairs.

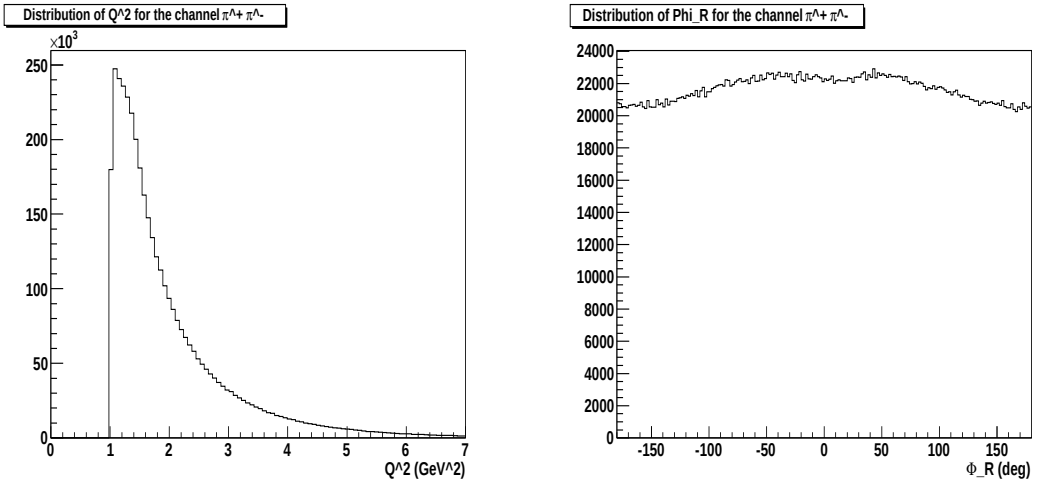

Figure 30: The Q^2-distribution of pion pairs (left) and the ϕ_R-distribution of the pair (right).

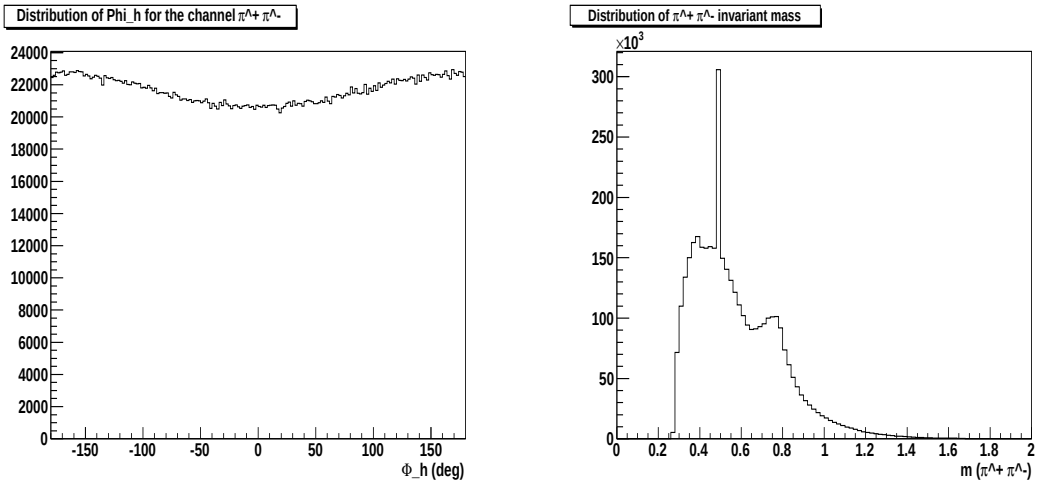

Figure 31: The $\phi_h$distribution (left) and invariant mass distributions of the pair (right).

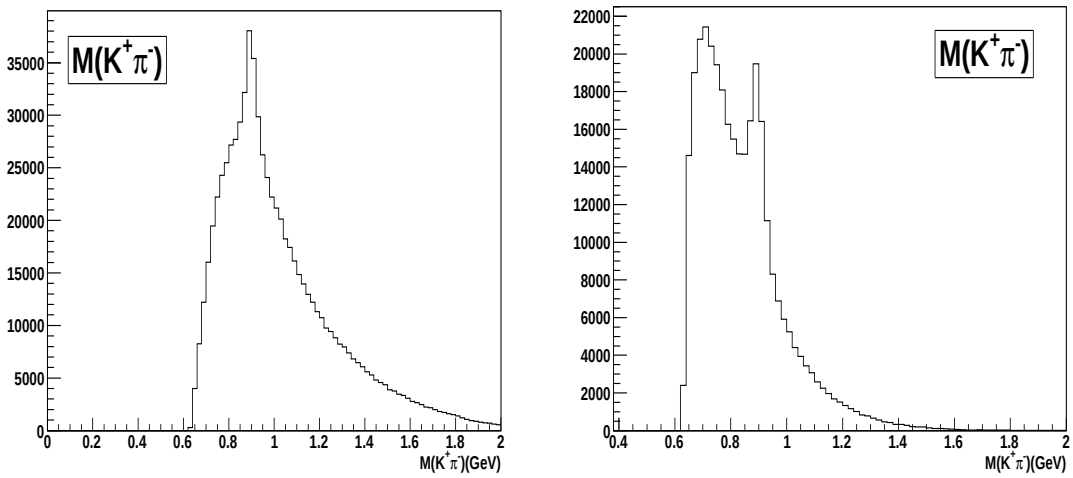

Figure 32: Invariant masses for Kaon-pion pairs for tfr-cfr and cfr-cfr combinations

Table 3: Uncertainties for asymmetry measurements.

Item	$A_{LU}^{\sin\phi}$	$A_{UL}^{\sin\phi}$
beam polarization	3%	-
target polarization	-	3%
dilution factor	-	4%
radiative corrections	2%	2%
fitting procedure	5%	5%
transverse (to γ^*) spin effects	-	3%

the measured SSA. For the $A_{UL}^{\sin\phi}$ SSA, statistical uncertainties are expected to dominate the total uncertainty.

Studies of other sources of systematics, related to physics background, including target fragmentation, semi-exclusive processes, exclusive vector meson contributions, and higher twist require the data of this measurement.

We based our predicted statistical errors for unpolarized target asymmetries in the following sections on the assumption of running 54 days on a hydrogen and deuterium [141]. Predicted statistical errors for polarized target SSA assume running 30 days on NH_3 and 50 days on ND_3. The number of days was chosen to achieve a statistical error that is not significantly larger than the systematical error at the highest x and M_h points. More days on deuterium than the proton ensures that both have the same statistical error at large P_T and optimizes the error on extracted $h_L^{u,d}$.

For our estimate of the total systematic error, we have added the systematic errors from the various contributions in quadrature. They are listed in Table 3. Note that some systematic errors (like the overall scale error coming from the beam and target polarization) affect the extraction of higher twist contributions less than point-to-point errors, which typically are smaller. Additional contributions to systematic error of measured asymmetries will come from uncertainties of unpolarized structure functions and also attenuation of hadrons

in nuclear environment, which are a subject of a separate study (PAC-30 proposal on nuclei).

7.3 Results

The proposed experiment will collect data on semi-inclusive electroproduction of hadron pairs including all combinations of kaons and pions with unpolarized and longitudinally polarized hydrogen and deuterium targets. The charged kaons will be detected in the forward spectrometer and the central tracker of CLAS12 in coincidence with the scattered electrons and identified by the CLAS12-RICH detector. The following predicted results were obtained with a full simulation of the hadronization process [151] and the acceptance of CLAS12 for all particles.

The expected counts of pion-pion and pion-kaons pairs in different kinematic bins for unpolarized and longitudinally polarized hydrogen and deuteron targets were calculated using the PEPSI-MC.

Projections for the resulting kinematic dependence of the beam SSA for proton target are shown in Fig. 33 for $\pi^+\pi^-$ pairs, in Fig. 34 for $K^+\pi^-$ pairs and in Fig. 35 for $K^+\pi^0$ pairs,respectively. The Fig. 37 shows the same SSA $\pi^+\pi^-$ for the deuteron target. Error bands represent upper and lower limits of different model calculations shown in Fig. 7, Fig. 11, and Fig. 9.

Projections for the resulting kinematic dependence of the twist-3 target SSA for proton and deuteron are shown in Fig. 36 and Fig. 38, respectively. Error bands represent upper and lower limits of different model calculations shown in Fig. 8 and Fig. 10.

The new data will also allow a more precise test of the factorization ansatz and the investigation of the Q^2 dependence of $\sin\phi$, and $\cos\phi$ asymmetries. This will enable us to study the higher-twist nature of the corresponding observables [152, 76, 153, 40, 39, 154, 155].

The combined analysis of the future `CLAS12` data on $\langle\sin\phi\rangle$ and of the previous HERMES measurements in the high-Q^2 domain (where higher-twist effects should be less significant) will provide information on the underlying quark-gluon correlations.

Measurements of spin and azimuthal asymmetries across a wide range of x, z, Q^2, and M_h would allow to perform detailed tests of QCD dynamics in valence region.

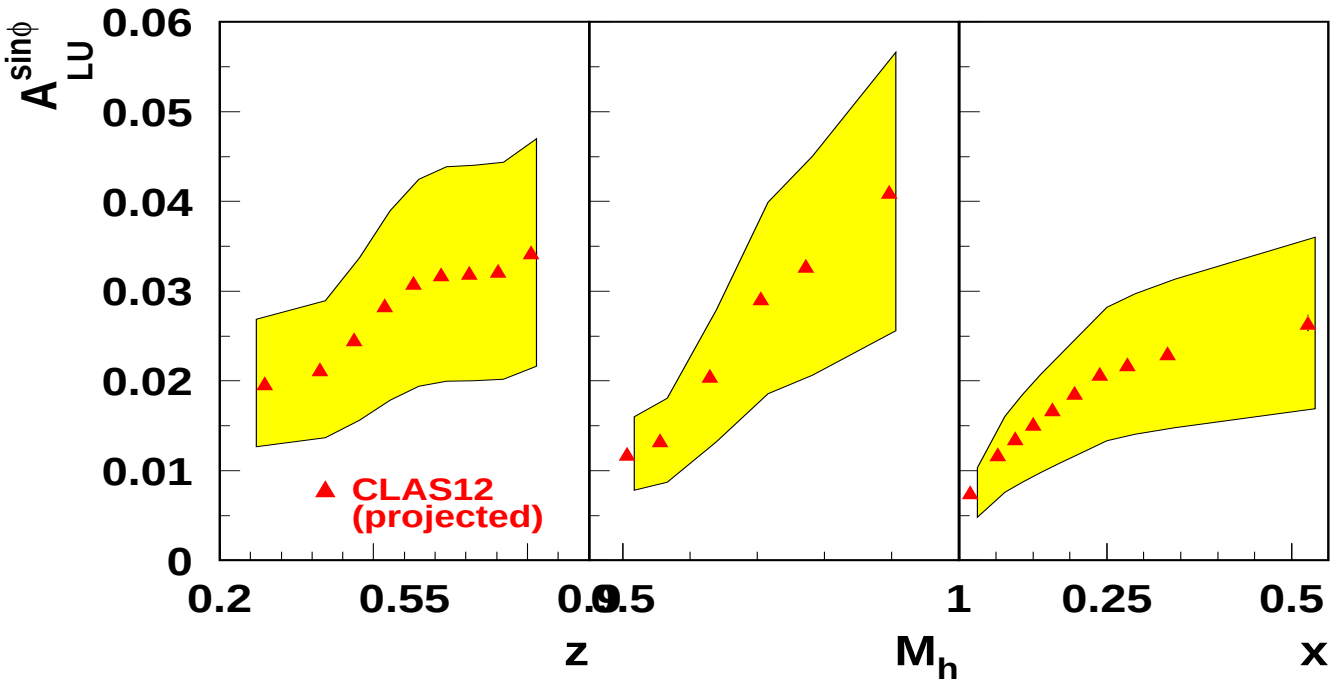

Figure 33: The projected statistical error for hydrogen target for the beam asymmetry $A_{LU}^{\sin\phi_R \sin\theta}$ in (z, M_h, x) for $\pi^+\pi^-$ pairs. The band represent the spread in predictions for two different models for $e(x)$ from Fig. 7.

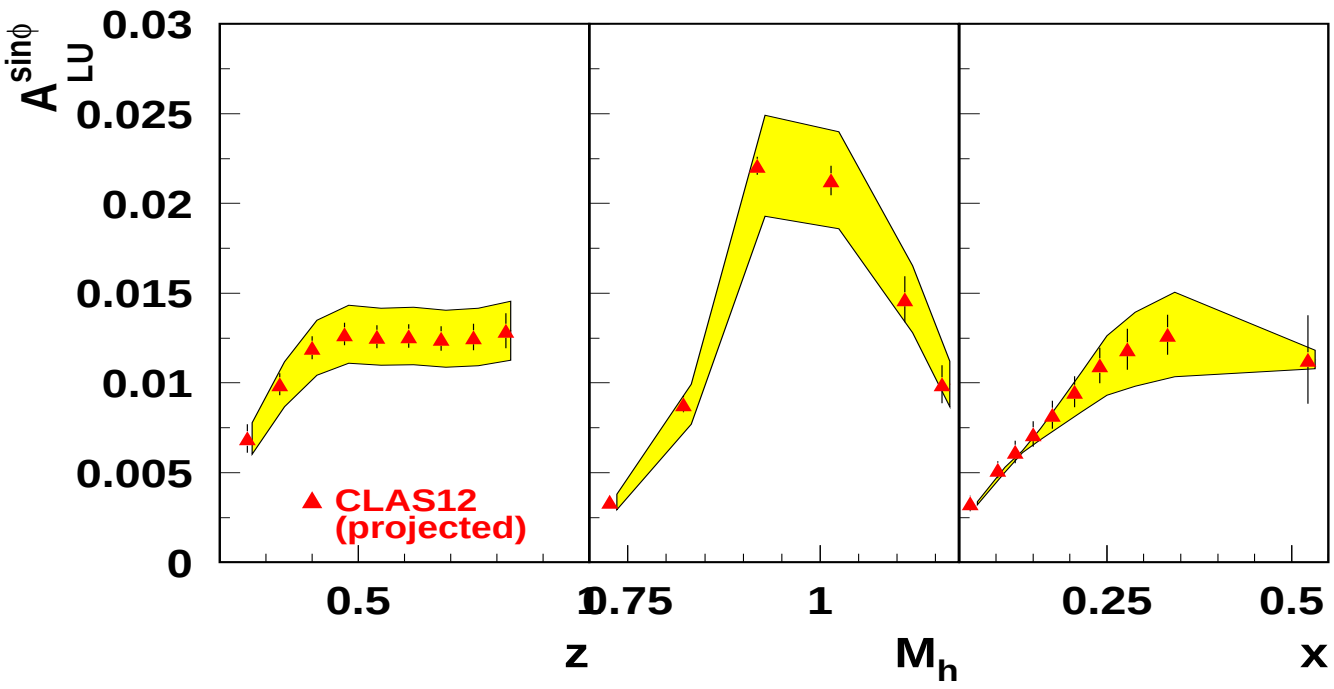

Figure 34: The projected statistical error for hydrogen target for the beam asymmetry $A_{LU}^{\sin\phi_R \sin\theta}$ in (z, M_h, x) for $K^+\pi^-$ pairs. The band represent the spread in predictions for two different models for $e(x)$ from Fig. 11.

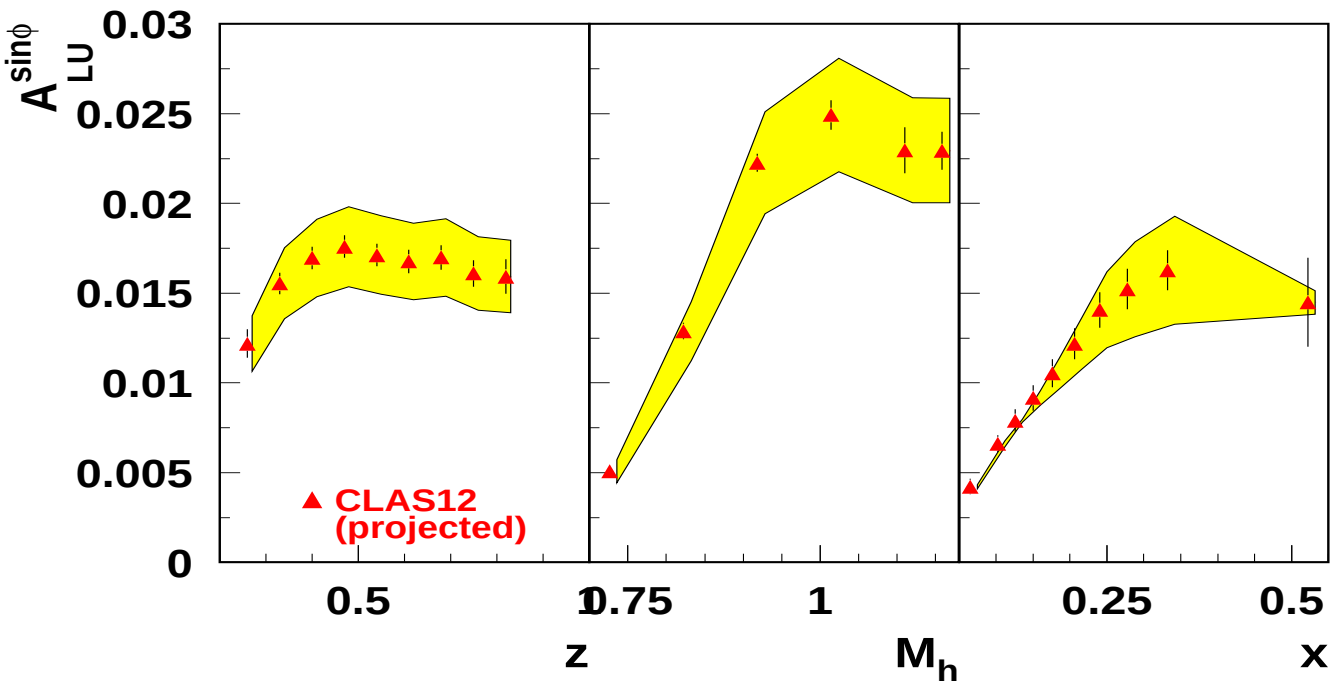

Figure 35: The projected statistical error for hydrogen target for the beam asymmetry $A_{LU}^{\sin\phi_R \sin\theta}$ in (z, M_h, x) for $K^+\pi^0$ pairs. The band represent the spread in predictions for two different models for $e(x)$ from Fig. 11.

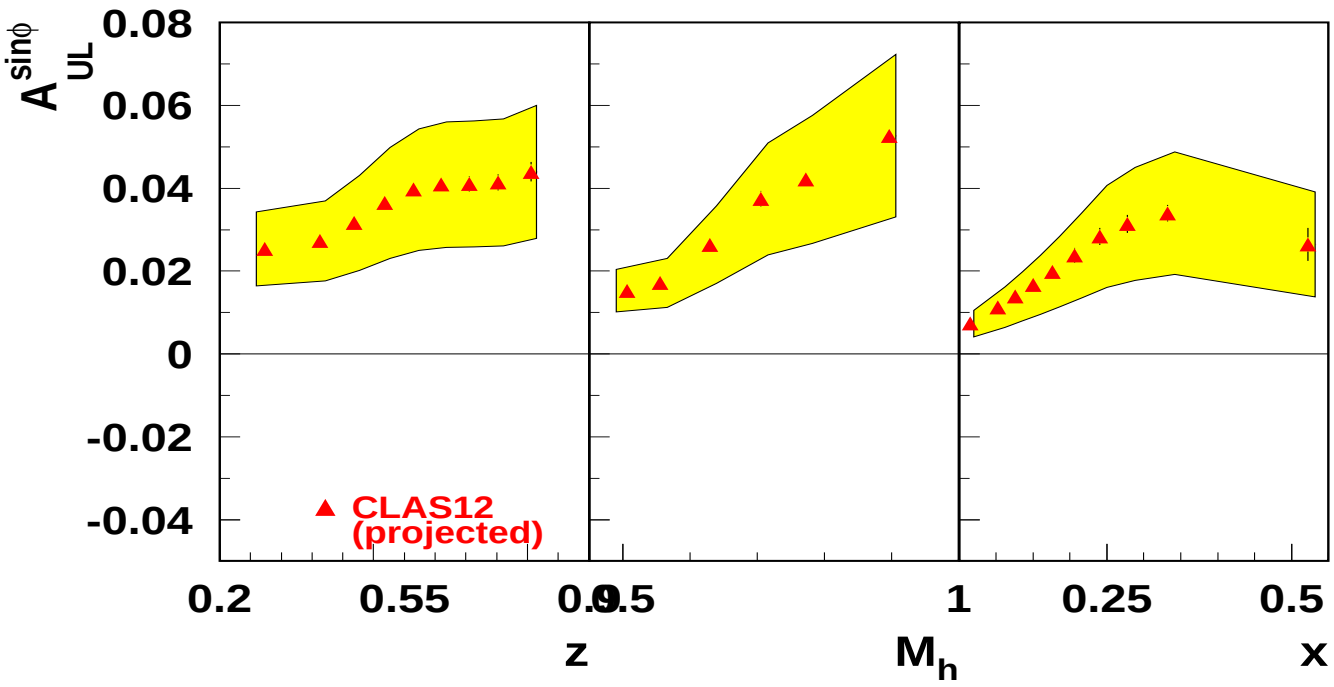

Figure 36: The projected statistical error for hydrogen target (30 days of NH_3) for the target asymmetry $A_{UL}^{\sin\phi_R \sin\theta}$ in (z, M_h, x). The band represent the spread in predictions for two different models for $h_L(x)$ from Fig. 8.

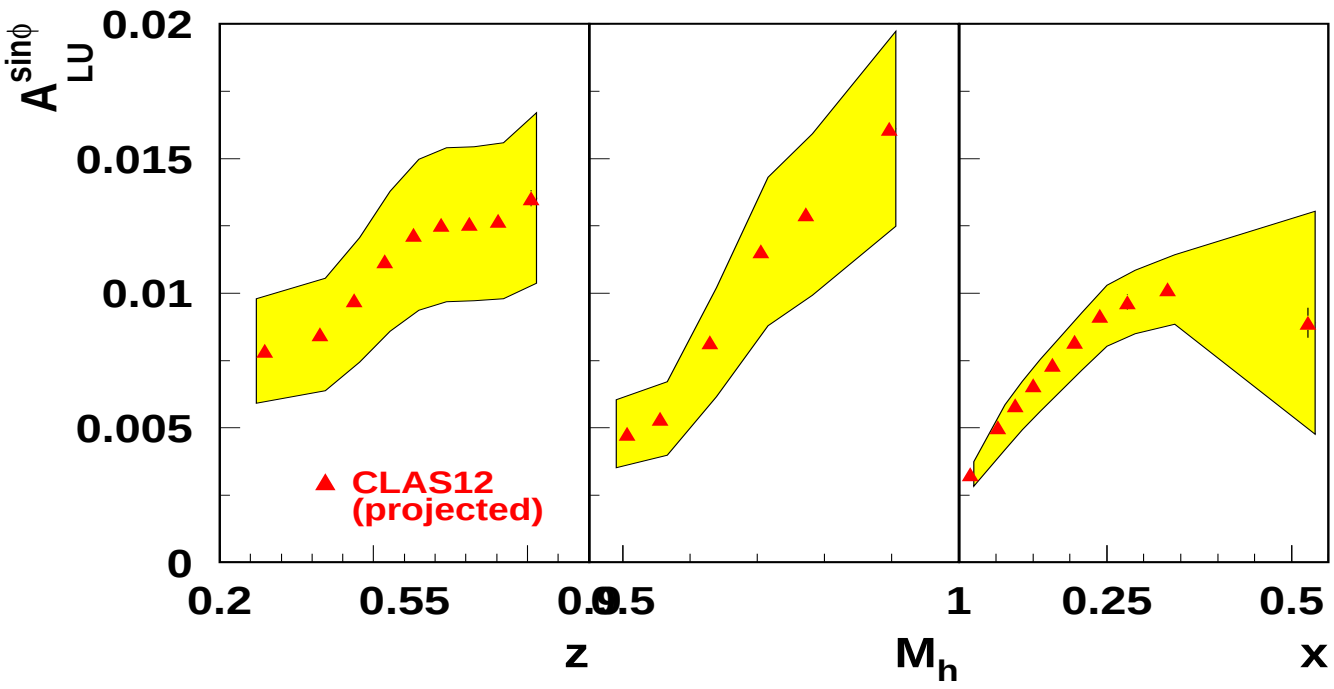

Figure 37: The projected statistical error for deuteron target (54 days) for the beam asymmetry $A_{LU}^{\sin\phi_R \sin\theta}$ in (z, M_h, x). The band represent the spread in predictions for two different models for $e(x)$ from Fig. 9.

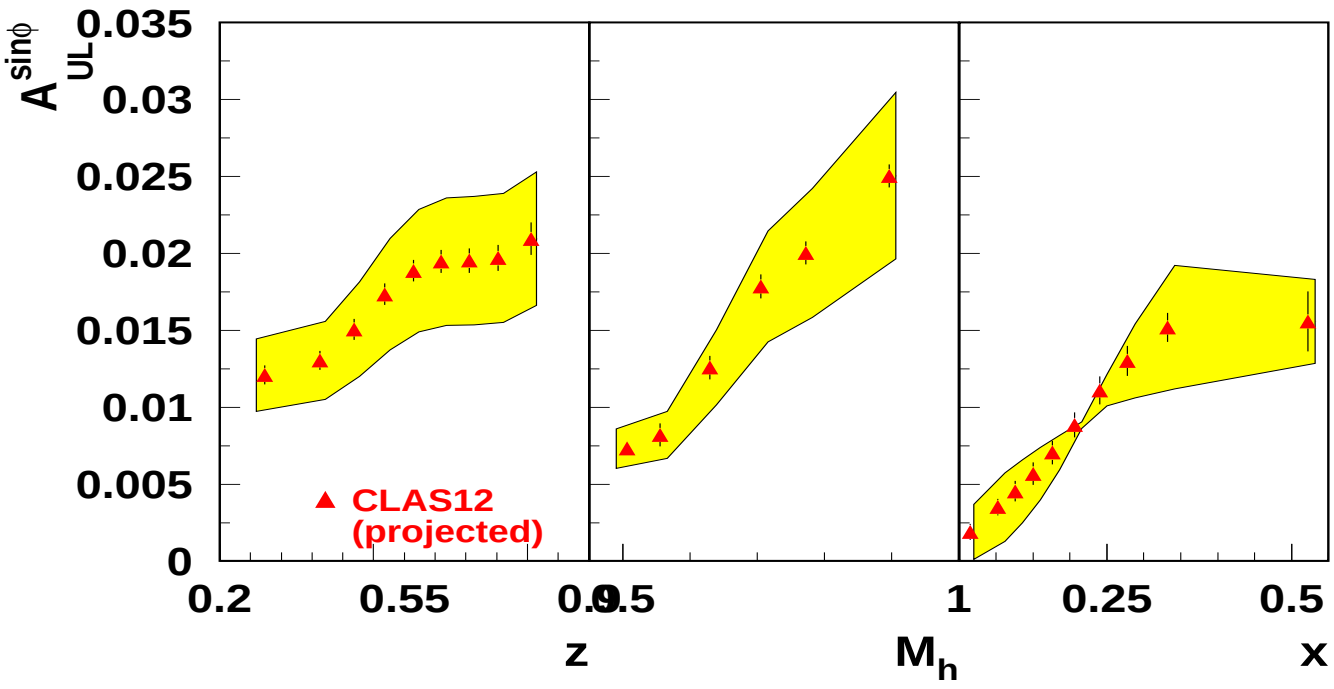

Figure 38: The projected statistical error for deuteron target (50 days of ND_3) for the target asymmetry $A_{UL}^{\sin\phi_R \sin\theta}$ in (z, M_h, x). The band represent the spread in predictions for two different models for $h_L(x)$ from Fig. 10.

8 Summary and Request

In recent years significant experimental, phenomenological and theoretical efforts have been made to understand the QCD beyond twist-2. Twist-3 functions describing multiparton distributions corresponding to the interference of higher Fock components in the hadron wave functions, offer fascinating insights into the nucleon structure [24].

The main goal of the proposal is to extract information on the twist-3 collinear pdfs $e(x)$ and $h_L(x)$, using the recent progress in understanding of DiFF and their extraction from e+e- data. The formalism of DiFFs is based on collinear factorization with well defined evolution equations. The proposed experiment will provide data on sub-leading asymmetries which would provide valuable insights, and especially provide an answer to the interesting question why subleading twist effects appear to be larger then leading twist effects ($A_{UU}^{\cos\phi}$ was larger than $A_{UU}^{\cos 2\phi}$ [16], $A_{UL}^{\sin\phi}$ was larger than $A_{UL}^{\sin 2\phi}$ [1]). Precise data on the production of pion and kaon pairs would have an important impact, and motivate further theoretical studies. Ultimately, through a global study of all of these observables, one could simultaneously obtain better knowledge of twist-3 collinear functions and twist-2 TMDs, and at the same time test the validity of the formalism. The proposed set of measurements with unpolarized and longitudinally polarized proton and deuteron targets will yield a comprehensive set of azimuthal moments in spin-dependent and independent SIDIS providing access to corresponding distribution and fragmentation functions in a wide range of x, Q^2, z, and M_h. Our data, combined with the data from HERMES, COMPASS, and BELLE, will provide independent (complementary to $e+/e-$) measurement of polarized and unpolarized pion and kaon DiFFs and will allow a complementary to pion SIDIS study of leading twist distributions.

To achieve this goal, we request a total of 164 days of beam time with an 11 GeV, highly polarized electron beam in Hall B with luminosity of $10^{35}\text{cm}^{-2}\text{sec}^{-1}$, including 108 days of polarized target running and 56 days of unpolarized target running. The breakdown of this beam time is shown in Table 4.

We want to conclude by noting that while this proposed experiments requires a substantial commitment of beam time (164 days total), we will simultaneously take data with already approved experiments to study the inclusive and semi-inclusive DIS [139, 131].

Time	Activity
Unpolarized target	
2 days	Commissioning: Empty target, interchange of targets
54 days	Production data taking on proton and deuterium (50% with reversed field)
Polarized target	
3 days	Commissioning: Beam raster set up, trigger optimization, low energy calibration runs
30 days	Production data taking on NH_3
50 days	Production data taking on ND_3
3 days (1 1/2 hours every other day)	Target anneals and/or target changes
15 days (intermittent with production data)	Calibration runs on ^{12}C and empty target
5 days	Production runs on ^{15}N
2 day (1 hour every other day – concurrent with anneals)	Möller polarimeter runs

Table 4: Requested beam time broken down by activity.

9 Appendix-A

The depolarization factors from Eq.2 can be written as

$$\frac{y^2}{2\,(1-\varepsilon)} = \frac{1}{1+\gamma^2}\left(1-y+\tfrac{1}{2}y^2+\tfrac{1}{4}\gamma^2y^2\right) \approx \left(1-y+\tfrac{1}{2}y^2\right) \equiv A(y), \tag{88}$$

$$\frac{y^2}{2\,(1-\varepsilon)}\,\varepsilon = \frac{1}{1+\gamma^2}\left(1-y-\tfrac{1}{4}\gamma^2y^2\right) \approx (1-y) \equiv B(y), \tag{89}$$

$$\frac{y^2}{2\,(1-\varepsilon)}\,\sqrt{2\,\varepsilon(1+\varepsilon)} = \frac{1}{1+\gamma^2}\,(2-y)\,\sqrt{1-y-\tfrac{1}{4}\gamma^2y^2} \approx (2-y)\,\sqrt{1-y} \equiv V(y), \tag{90}$$

$$\frac{y^2}{2\,(1-\varepsilon)}\,\sqrt{2\,\varepsilon(1-\varepsilon)} = \frac{1}{\sqrt{1+\gamma^2}}\,y\,\sqrt{1-y-\tfrac{1}{4}\gamma^2y^2} \approx y\,\sqrt{1-y} \equiv W(y), \tag{91}$$

$$\frac{y^2}{2\,(1-\varepsilon)}\,\sqrt{1-\varepsilon^2} = \frac{1}{\sqrt{1+\gamma^2}}\,y\left(1-\tfrac{1}{2}y\right) \approx y\left(1-\tfrac{1}{2}y\right) \equiv C(y). \tag{92}$$

10 Appendix-B

For an arbitrary function $w(\mathbf{k},\mathbf{p})$ we introduce the notation

$$C[\hat{M}\cdot D\,w] = \sum_a e_a^2 \int d^2\mathbf{k}\,d^2\mathbf{p}\,\delta^{(2)}(z\mathbf{k}+\mathbf{p}-\mathbf{P}_{T1})\,\hat{M}_a(x,\zeta,\mathbf{k}^2,\mathbf{P}_{T2}^2,\mathbf{k}\cdot\mathbf{P}_{T2})D_a(z,\mathbf{p}^2)\,w, \tag{93}$$

where $\mathbf{k},\mathbf{P}_{T1}$ and $\mathbf{P}_{T2}$ are the two-dimensional transverse momenta of quark, hadrons 1 and 2 with respect to virtual photon momentum and $\mathbf{p}$ is a hadron 1 transverse momentum with respect to fragmenting quark momentum. Then, using the identity for Kronecker delta-function in two-dimensional vectors space

$$\left(\mathbf{P}_{T1}^2\mathbf{P}_{T2}^2-(\mathbf{P}_{T1}\cdot\mathbf{P}_{T2})^2\right)\delta^{ij} = \mathbf{P}_{T2}^2P_{T1}^iP_{T1}^j+\mathbf{P}_{T1}^2P_{T2}^iP_{T2}^j-(\mathbf{P}_{T1}\cdot\mathbf{P}_{T2})\left(P_{T1}^iP_{T2}^j+P_{T1}^jP_{T2}^i\right), \tag{94}$$

we have the following general tensorial decomposition over independent structures:

$$\begin{aligned}
C[\hat{M}\cdot D] &= F_0^{\hat{M}\cdot D}\,,\\
C[\hat{M}\cdot D\,k^i] &= P_{T1}^i\,F_{k1}^{\hat{M}\cdot D}+P_{T2}^i\,F_{k2}^{\hat{M}\cdot D}\,,\\
C[\hat{M}\cdot D\,p^i] &= P_{T1}^i\,F_{p1}^{\hat{M}\cdot D}+P_{T2}^i\,F_{p2}^{\hat{M}\cdot D}\,,\\
C[\hat{M}\cdot D\,k^ik^j] &= P_{T1}^iP_{T1}^j\,F_{kk1}^{\hat{M}\cdot D}+P_{T2}^iP_{T2}^j\,F_{kk2}^{\hat{M}\cdot D}+\delta^{ij}\,F_{kk3}^{\hat{M}\cdot D}\,,\\
C[\hat{M}\cdot D\,k^ip^j] &= P_{T1}^iP_{T1}^j\,F_{kp1}^{\hat{M}\cdot D}+P_{T2}^iP_{T2}^j\,F_{kp2}^{\hat{M}\cdot D}+\left(P_{T1}^iP_{T2}^j-P_{T1}^jP_{T2}^i\right)\,F_{kp3}^{\hat{M}\cdot D}+\delta^{ij}\,F_{kp4}^{\hat{M}\cdot D}\,,\\
C[\hat{M}\cdot D\,k^ik^jp^k] &= P_{T1}^iP_{T1}^jP_{T1}^k\,F_{kkp1}^{\hat{M}\cdot D}+P_{T1}^iP_{T1}^jP_{T2}^k\,F_{kkp2}^{\hat{M}\cdot D}+P_{T2}^iP_{T2}^jP_{T2}^k\,F_{kkp3}^{\hat{M}\cdot D}+P_{T2}^iP_{T2}^jP_{T1}^k\,F_{kkp4}^{\hat{M}\cdot D}\\
&+ P_{T1}^k\delta^{ij}\,F_{kkp5}^{\hat{M}\cdot D}+P_{T2}^k\delta^{ij}\,F_{kkp6}^{\hat{M}\cdot D}\,.
\end{aligned} \tag{95}$$

Note, that the functions in the r.h.s. of above equations depend on $x,z,\zeta,\mathbf{P}_{T1}^2,\mathbf{P}_{T2}^2,\mathbf{P}_{T1}\cdot\mathbf{P}_{T2}$.

From Eq.(95), after contracting by appropriate tensorial combinations, constructed from components of $\mathbf{P}_{T1}$ and $\mathbf{P}_{T2}$ and δ^{ij}, we can easily obtain

$$\begin{aligned} F_{k1}^{\hat{M}\cdot D} &= C\left[\hat{M}\cdot D\frac{(\mathbf{P}_{T1}\cdot\mathbf{P}_{T2})(\mathbf{P}_{T2}\cdot\mathbf{k})-(\mathbf{P}_{T1}\cdot\mathbf{k})\mathbf{P}_{T2}^2}{(\mathbf{P}_{T1}\cdot\mathbf{P}_{T2})^2-\mathbf{P}_{T1}^2\mathbf{P}_{T2}^2}\right], \\ F_{k2}^{\hat{M}\cdot D} &= C\left[\hat{M}\cdot D\frac{(\mathbf{P}_{T1}\cdot\mathbf{k})(\mathbf{P}_{T1}\cdot\mathbf{P}_{T2})-(\mathbf{P}_{T2}\cdot\mathbf{k})\mathbf{P}_{T1}^2}{(\mathbf{P}_{T1}\cdot\mathbf{P}_{T2})^2-\mathbf{P}_{T1}^2\mathbf{P}_{T2}^2}\right]. \end{aligned} \tag{96}$$

$$\begin{aligned} F_{p1}^{\hat{M}\cdot D} &= C\left[\hat{M}\cdot D\frac{(\mathbf{P}_{T1}\cdot\mathbf{P}_{T2})(\mathbf{P}_{T2}\cdot\mathbf{p})-(\mathbf{P}_{T1}\cdot\mathbf{p})\mathbf{P}_{T2}^2}{(\mathbf{P}_{T1}\cdot\mathbf{P}_{T2})^2-\mathbf{P}_{T1}^2\mathbf{P}_{T2}^2}\right], \\ F_{p2}^{\hat{M}\cdot D} &= C\left[\hat{M}\cdot D\frac{(\mathbf{P}_{T1}\cdot\mathbf{p})(\mathbf{P}_{T1}\cdot\mathbf{P}_{T2})-(\mathbf{P}_{T2}\cdot\mathbf{p})\mathbf{P}_{T1}^2}{(\mathbf{P}_{T1}\cdot\mathbf{P}_{T2})^2-\mathbf{P}_{T1}^2\mathbf{P}_{T2}^2}\right]. \end{aligned} \tag{97}$$

$$\begin{aligned} F_{kk1}^{\hat{M}\cdot D} &= C\left[\hat{M}\cdot D\,\frac{\left(-2\left(\mathbf{P}_{T1}\cdot\mathbf{k}\right)^2+\mathbf{k}^2\mathbf{P}_{T1}^2\right)\mathbf{P}_{T2}^4+\left(2\left(\mathbf{P}_{T2}\cdot\mathbf{k}\right)^2-\mathbf{k}^2\mathbf{P}_{T2}^2\right)\left(2\left(\mathbf{P}_{T1}\cdot\mathbf{P}_{T2}\right)^2-\mathbf{P}_{T1}^2\mathbf{P}_{T2}^2\right)}{4\left(\mathbf{P}_{T1}\cdot\mathbf{P}_{T2}\right)^2\left(\left(\mathbf{P}_{T1}\cdot\mathbf{P}_{T2}\right)^2-\mathbf{P}_{T1}^2\mathbf{P}_{T2}^2\right)}\right], \\ F_{kk2}^{\hat{M}\cdot D} &= C\left[\hat{M}\cdot D\,\frac{\left(2\left(\mathbf{P}_{T1}\cdot\mathbf{P}_{T2}\right)^2-\mathbf{P}_{T1}^2\mathbf{P}_{T2}^2\right)\left(\mathbf{P}_{T1}\cdot\mathbf{k}\right)^2+\mathbf{P}_{T1}^2\left(\mathbf{P}_{T1}^2\mathbf{P}_{T2}^2-\left(\mathbf{P}_{T1}\cdot\mathbf{P}_{T2}\right)^2\right)\mathbf{k}^2-\left(\mathbf{P}_{T2}\cdot\mathbf{k}\right)^2}{2\left(\mathbf{P}_{T1}\cdot\mathbf{P}_{T2}\right)^2\left(\left(\mathbf{P}_{T1}\cdot\mathbf{P}_{T2}\right)^2-\mathbf{P}_{T1}^2\mathbf{P}_{T2}^2\right)}\right], \\ F_{kk3}^{\hat{M}\cdot D} &= C\left[\hat{M}\cdot D\,\frac{\left(\left(\mathbf{P}_{T1}\cdot\mathbf{P}_{T2}\right)^2+\mathbf{P}_{T1}^2\mathbf{P}_{T2}^2\right)\mathbf{k}^2-\left(\mathbf{P}_{T2}\cdot\mathbf{k}\right)^2\mathbf{P}_{T1}^2-\left(\mathbf{P}_{T1}\cdot\mathbf{k}\right)^2\mathbf{P}_{T2}^2}{2\left(\mathbf{P}_{T1}\cdot\mathbf{P}_{T2}\right)^2}\right]. \end{aligned}$$

$$\begin{aligned} F_{kp1}^{\hat{M}\cdot D} &= C\left[\hat{M}\cdot D\left(\frac{\left(-2(\mathbf{P}_{T1}\cdot\mathbf{k})(\mathbf{P}_{T1}\cdot\mathbf{p})+(\mathbf{k}\cdot\mathbf{p})\mathbf{P}_{T1}^2\right)\mathbf{P}_{T2}^4}{4\left(\mathbf{P}_{T1}\cdot\mathbf{P}_{T2}\right)^2\left(\left(\mathbf{P}_{T1}\cdot\mathbf{P}_{T2}\right)^4-\mathbf{P}_{T1}^2\mathbf{P}_{T2}^2\right)}+\right.\right. \\ &\qquad\left.\left.\frac{(2(\mathbf{P}_{T2}\cdot\mathbf{k})(\mathbf{P}_{T2}\cdot\mathbf{p})-(\mathbf{k}\cdot\mathbf{p})\mathbf{P}_{T2}^2)\left(2\left(\mathbf{P}_{T1}\cdot\mathbf{P}_{T2}\right)^2-\mathbf{P}_{T1}^2\mathbf{P}_{T2}^2\right)}{4\left(\mathbf{P}_{T1}\cdot\mathbf{P}_{T2}\right)^2\left(\left(\mathbf{P}_{T1}\cdot\mathbf{P}_{T2}\right)^4-\mathbf{P}_{T1}^2\mathbf{P}_{T2}^2\right)}\right)\right], \\ F_{kp2}^{\hat{M}\cdot D} &= C\left[\hat{M}\cdot D\left(\frac{\left(\mathbf{P}_{T1}\cdot\mathbf{k}\right)\left(\mathbf{P}_{T1}\cdot\mathbf{p}\right)\left(2\left(\mathbf{P}_{T1}\cdot\mathbf{P}_{T2}\right)^2-\mathbf{P}_{T1}^2\mathbf{P}_{T2}^2\right)}{2\left(\mathbf{P}_{T1}\cdot\mathbf{P}_{T2}\right)^2\left(\left(\mathbf{P}_{T1}\cdot\mathbf{P}_{T2}\right)^2-\mathbf{P}_{T1}^2\mathbf{P}_{T2}^2\right)}-\right.\right. \\ &\qquad\left.\left.\frac{\left(\mathbf{P}_{T2}\cdot\mathbf{k}\right)\left(\mathbf{P}_{T2}\cdot\mathbf{p}\right)\mathbf{P}_{T1}^4+\left(\mathbf{k}\cdot\mathbf{p}\right)\mathbf{P}_{T1}^2\left(\mathbf{P}_{T1}^2\mathbf{P}_{T2}^2-\left(\mathbf{P}_{T1}\cdot\mathbf{P}_{T2}\right)^2\right)}{2\left(\mathbf{P}_{T1}\cdot\mathbf{P}_{T2}\right)^2\left(\left(\mathbf{P}_{T1}\cdot\mathbf{P}_{T2}\right)^2-\mathbf{P}_{T1}^2\mathbf{P}_{T2}^2\right)}\right)\right], \\ F_{kp3}^{\hat{M}\cdot D} &= C\left[\hat{M}\cdot D\,\frac{\left(\mathbf{P}_{T1}\cdot\mathbf{k}\right)\left(\mathbf{P}_{T2}\cdot p\right)-\left(\mathbf{P}_{T1}\cdot\mathbf{p}\right)\left(\mathbf{P}_{T2}\cdot\mathbf{k}\right)}{2\left(\mathbf{P}_{T1}^2\mathbf{P}_{T2}^2-\left(\mathbf{P}_{T1}\cdot\mathbf{P}_{T2}\right)^2\right)}\right], \\ F_{kp4}^{\hat{M}\cdot D} &= C\left[\hat{M}\cdot D\,\frac{\left(\mathbf{k}\cdot\mathbf{p}\right)\left(\left(\mathbf{P}_{T1}\cdot\mathbf{P}_{T2}\right)^2+\mathbf{P}_{T1}^2\mathbf{P}_{T2}^2\right)-\left(\mathbf{P}_{T2}\cdot\mathbf{k}\right)\left(\mathbf{P}_{T2}\cdot\mathbf{p}\right)\mathbf{P}_{T1}^2-\left(\mathbf{P}_{T1}\cdot\mathbf{k}\right)\left(\mathbf{P}_{T1}\cdot\mathbf{p}\right)\mathbf{P}_{T2}^2}{2\left(\mathbf{P}_{T1}\cdot\mathbf{P}_{T2}\right)^2}\right] \end{aligned} \tag{99}$$

References

[1] HERMES, A. Airapetian et al., Phys. Rev. Lett. 84 (2000) 4047, hep-ex/9910062.

[2] HERMES, A. Airapetian et al., Phys. Rev. D64 (2001) 097101, hep-ex/0104005.

[3] HERMES, A. Airapetian et al., Phys. Rev. Lett. 94 (2005) 012002, hep-ex/0408013.

[4] HERMES, A. Airapetian et al., Phys. Lett. B648 (2007) 164, hep-ex/0612059.

[5] COMPASS, V.Y. Alexakhin et al., Phys. Rev. Lett. 94 (2005) 202002, hep-ex/0503002.

[6] CLAS, H. Avakian et al., Phys. Rev. D69 (2004) 112004, hep-ex/0301005.

[7] CLAS, H. Avakian et al., AIP Conf. Proc. 792 (2005) 945, nucl-ex/0509032.

[8] H. Mkrtchyan et al., Phys. Lett. B665 (2008) 20, hep-ph/0709.3020.

[9] CLAS, M. Osipenko et al., Phys. Rev. D80 (2009) 032004, hep-ex/0809.1153.

[10] STAR, J. Adams et al., Phys. Rev. Lett. 92 (2004) 171801, hep-ex/0310058.

[11] PHENIX, M. Chiu, AIP Conf. Proc. 915 (2007) 539, nucl-ex/0701031.

[12] BRAHMS, I. Arsene et al., Phys. Rev. Lett. 101 (2008) 042001, nucl-ex/0801.1078.

[13] Belle, K. Abe et al., Phys. Rev. Lett. 96 (2006) 232002, hep-ex/0507063.

[14] BELLE Collaboration, A. Vossen et al., Phys.Rev.Lett. (2011), 1104.2425.

[15] European Muon, J.J. Aubert et al., Phys. Lett. B130 (1983) 118.

[16] European Muon, M. Arneodo et al., Z. Phys. C34 (1987) 277.

[17] COMPASS, W. Kafer, Transversity 2008 proceedings (2008), hep-ex/0808.0114.

[18] HERMES, F. Giordano and R. Lamb, AIP Conf. Proc. 1149 (2009) 423, hep-ex/0901.2438.

[19] COMPASS, G. Sbrizzai, (2009), 0902.0578.

[20] W. Gohn et al., AIP Conf. Proc. 1149 (2009) 461.

[21] HERMES, A. Airapetian et al., Phys. Lett. B562 (2003) 182, hep-ex/0212039.

[22] HERMES, A. Airapetian et al., Phys. Lett. B622 (2005) 14, hep-ex/0505042.

[23] R.L. Jaffe, Comments Nucl. Part. Phys. 19 (1990) 239.

[24] M. Burkardt, (2008), hep-ph/0810.3589.

[25] The CLAS, H. Avakian et al., Phys. Rev. Lett. 105 (2010) 262002, hep-ex/1003.4549.

[26] M.G. Alekseev et al., Eur. Phys. J. C70 (2010) 39, 1007.1562.

[27] M. Anselmino and F. Murgia, Phys. Lett. B483 (2000) 74, hep-ph/0002120.

[28] E. De Sanctis, W.D. Nowak and K.A. Oganesian, Phys. Lett. B483 (2000) 69, hep-ph/0002091.

[29] A.V. Efremov et al., Phys. Lett. B478 (2000) 94, hep-ph/0001119.

[30] K.A. Oganessian et al., Nucl. Phys. A689 (2001) 784, hep-ph/0010261.

[31] A.V. Efremov, K. Goeke and P. Schweitzer, Phys. Lett. B522 (2001) 37, hep-ph/0108213.

[32] A.V. Efremov, K. Goeke and P. Schweitzer, Eur. Phys. J. C24 (2002) 407, hep-ph/0112166.

[33] A.V. Efremov, K. Goeke and P. Schweitzer, Eur. Phys. J. C32 (2003) 337, hep-ph/0309209.

[34] P. Schweitzer and A. Bacchetta, Nucl. Phys. A732 (2004) 106, hep-ph/0310318.

[35] A.V. Efremov, K. Goeke and P. Schweitzer, Phys. Lett. B568 (2003) 63, hep-ph/0303062.

[36] B.Q. Ma, I. Schmidt and J.J. Yang, Phys. Rev. D65 (2002) 034010, hep-ph/0110324.

[37] A.V. Efremov, K. Goeke and P. Schweitzer, Phys. Rev. D67 (2003) 114014, hep-ph/0208124.

[38] U. D'Alesio and F. Murgia, Phys.Rev. D70 (2004) 074009, hep-ph/0408092.

[39] F. Yuan, Phys. Lett. B589 (2004) 28, hep-ph/0310279.

[40] A. Afanasev and C.E. Carlson, (2003), hep-ph/0308163.

[41] A. Bacchetta, P.J. Mulders and F. Pijlman, Phys. Lett. B595 (2004) 309, hep-ph/0405154.

[42] L.P. Gamberg et al., Phys. Lett. B639 (2006) 508, hep-ph/0604022.

[43] A. Bacchetta et al., JHEP 08 (2008) 023, hep-ph/0803.0227.

[44] R.L. Jaffe, X.m. Jin and J. Tang, Phys. Rev. Lett. 80 (1998) 1166, hep-ph/9709322.

[45] A. Bianconi et al., Phys. Rev. D62 (2000) 034008, hep-ph/9907475.

[46] M. Radici, R. Jakob and A. Bianconi, Phys. Rev. D65 (2002) 074031, hep-ph/0110252.

[47] A. Bacchetta and M. Radici, Phys. Rev. D67 (2003) 094002, hep-ph/0212300.

[48] A. Bacchetta and M. Radici, Phys. Rev. D69 (2004) 074026, hep-ph/0311173.

[49] A. Bacchetta and M. Radici, Phys. Rev. D74 (2006) 114007, hep-ph/0608037.

[50] F.A. Ceccopieri, M. Radici and A. Bacchetta, Phys. Lett. B650 (2007) 81, hep-ph/0703265.

[51] A. Bacchetta, A. Courtoy and M. Radici, (2011), 1104.3855.

[52] A. Bacchetta et al., JHEP 02 (2007) 093, hep-ph/0611265.

[53] A. Bacchetta et al., Phys. Rev. D70 (2004) 117504, hep-ph/0410050.

[54] HERMES, A. Airapetian et al., JHEP 06 (2008) 017, 0803.2367.

[55] M. Diehl and S. Sapeta, Eur. Phys. J. C41 (2005) 515, hep-ph/0503023.

[56] J. Zhou and A. Metz, Phys. Rev. Lett. 106 (2011) 172001, hep-ph/1101.3273.

[57] S. Wandzura and F. Wilczek, Phys. Lett. B72 (1977) 195.

[58] R.D. Tangerman and P.J. Mulders, (1994), hep-ph/9408305.

[59] P.J. Mulders and R.D. Tangerman, Nucl. Phys. B461 (1996) 197, hep-ph/9510301.

[60] H. Avakian et al., Phys. Rev. D77 (2008) 014023, hep-ph/0709.3253.

[61] A. Metz, P. Schweitzer and T. Teckentrup, (2008), hep-ph/0810.5212.

[62] R.L. Jaffe and X.D. Ji, Phys. Rev. D43 (1991) 724.

[63] A. Harindranath and W.M. Zhang, Phys. Lett. B408 (1997) 347, hep-ph/9706419.

[64] R. Kundu and A. Metz, Phys. Rev. D65 (2002) 014009, hep-ph/0107073.

[65] A. Accardi et al., JHEP 11 (2009) 093, 0907.2942.

[66] N. Christ and T.D. Lee, Phys. Rev. 143 (1966) 1310.

[67] J.R. Chen et al., Phys. Rev. Lett. 21 (1968) 1279.

[68] S. Rock et al., Phys. Rev. Lett. 24 (1970) 748.

[69] J.A. Appel et al., Phys. Rev. D1 (1970) 1285.

[70] M. Schlegel and A. Metz, AIP Conf. Proc. 1149 (2009) 543, 0902.0781.

[71] S. Gliske, PhD. thesis, http://www-hermes.desy.de/notes/pub/10-LIB/sgliske.10-003.sidis-vm.pdf.

[72] A. Bianconi et al., Phys. Rev. D62 (2000) 034009, hep-ph/9907488.

[73] A. Bacchetta et al., Phys. Rev. D79 (2009) 034029, 0812.0611.

[74] X. Artru and J.C. Collins, Z. Phys. C69 (1996) 277, hep-ph/9504220.

[75] P.J. Mulders and J. Rodrigues, (1996), hep-ph/9702280.

[76] R.L. Jaffe and X.D. Ji, Nucl. Phys. B375 (1992) 527.

[77] R.L. Jaffe and X.D. Ji, Phys. Rev. Lett. 67 (1991) 552.

[78] R.L. Jaffe, Phys. Rev. D21 (1980) 3215.

[79] T.P. Cheng, Phys. Rev. D38 (1988) 2869.

[80] S. Weinberg, Phys. Rev. Lett. 17 (1966) 616.

[81] T.P. Cheng and W.K. Tung, Phys. Rev. D3 (1971) 733.

[82] L.S. Brown, W.J. Pardee and R.D. Peccei, Phys. Rev. D4 (1971) 2801.

[83] J. Gasser, H. Leutwyler and M.E. Sainio, Phys. Lett. B253 (1991) 252.

[84] J. Gasser, H. Leutwyler and M.E. Sainio, Phys. Lett. B253 (1991) 260.

[85] T. Becher and H. Leutwyler, Eur. Phys. J. C9 (1999) 643, hep-ph/9901384.

[86] J. Gasser, H. Leutwyler and M.E. Sainio, In *Bad Honnef 1991, Proceedings, Pion-nucleon physics and the structure of the nucleon, vol. 1* 56-57.

[87] M.M. Pavan et al., PiN Newslett. 16 (2002) 110, hep-ph/0111066.

[88] M.G. Olsson and W.B. Kaufmann, PiN Newslett. 16 (2002) 382.

[89] J. Gasser, Ann. Phys. 136 (1981) 62.

[90] J. Gasser and H. Leutwyler, Phys. Rept. 87 (1982) 77.

[91] X.D. Ji, Phys. Rev. Lett. 74 (1995) 1071, hep-ph/9410274.

[92] S.J. Dong, J.F. Lagae and K.F. Liu, Phys. Rev. D54 (1996) 5496, hep-ph/9602259.

[93] H. Hellmann, Einfuhrung in die Quantenchemie (1937).

[94] R.P. Feynman, Phys. Rev. 56 (1939).

[95] D.B. Leinweber, A.W. Thomas and S.V. Wright, Phys. Lett. B482 (2000) 109, hep-lat/0001007.

[96] D.B. Leinweber, A.W. Thomas and R.D. Young, Phys. Rev. Lett. 92 (2004) 242002, hep-lat/0302020.

[97] R.D. Young and A.W. Thomas, Phys. Rev. D81 (2010) 014503, 0901.3310.

[98] S.J. Brodsky, F.J. Llanes-Estrada and A.P. Szczepaniak, (2007), 0710.0981.

[99] J. Kodaira and K. Tanaka, Prog. Theor. Phys. 101 (1999) 191, hep-ph/9812449.

[100] A.V. Efremov and P. Schweitzer, JHEP 08 (2003) 006, hep-ph/0212044.

[101] M. Burkardt, Phys. Rev. D52 (1995) 3841, hep-ph/9505226.

[102] M. Burkardt and Y. Koike, Nucl. Phys. B632 (2002) 311, hep-ph/0111343.

[103] P. Schweitzer, Phys. Rev. D67 (2003) 114010, hep-ph/0303011.

[104] M. Wakamatsu and Y. Ohnishi, Phys. Rev. D67 (2003) 114011, hep-ph/0303007.

[105] Y. Ohnishi and M. Wakamatsu, Phys. Rev. D69 (2004) 114002, hep-ph/0312044.

[106] C. Cebulla et al., Acta Phys. Polon. B39 (2008) 609, 0710.3103.

[107] P. Schweitzer, Phys. Rev. D69 (2004) 034003, hep-ph/0307336.

[108] M. Wakamatsu and H. Tsujimoto, (2009), 0910.5762.

[109] A.I. Signal, Nucl. Phys. B497 (1997) 415, hep-ph/9610480.

[110] R. Jakob, P.J. Mulders and J. Rodrigues, Nucl. Phys. A626 (1997) 937, hep-ph/9704335.

[111] A. Mukherjee, Phys. Lett. B687 (2010) 180, 0912.1446.

[112] S.J. Brodsky, F.E. Close and J.F. Gunion, Phys. Rev. D5 (1972) 1384.

[113] R.L. Jaffe and C.H. Llewellyn Smith, Phys. Rev. D7 (1973) 2506.

[114] D.J. Broadhurst, J.F. Gunion and R.L. Jaffe, Ann. Phys. 81 (1973) 88.

[115] H. Burkhardt and W.N. Cottingham, Annals Phys. 56 (1970) 453.

[116] S.D. Drell and A.C. Hearn, Phys. Rev. Lett. 16 (1966) 908.

[117] A.V. Efremov, O.V. Teryaev and E. Leader, Phys. Rev. D55 (1997) 4307, hep-ph/9607217.

[118] B. Dressler, M. Maul and C. Weiss, Nucl. Phys. B578 (2000) 293, hep-ph/9906444.

[119] P. Schweitzer et al., Phys. Rev. D64 (2001) 034013, hep-ph/0101300.

[120] D. Diakonov, Prog. Part. Nucl. Phys. 51 (2003) 173, hep-ph/0212026.

[121] D. Diakonov, M.V. Polyakov and C. Weiss, Nucl. Phys. B461 (1996) 539, hep-ph/9510232.

[122] I.I. Balitsky et al., Phys. Rev. Lett. 77 (1996) 3078, hep-ph/9605439.

[123] A.V. Belitsky and D. Mueller, Nucl. Phys. B503 (1997) 279, hep-ph/9702354.

[124] Y. Koike and N. Nishiyama, Phys. Rev. D55 (1997) 3068, hep-ph/9609207.

[125] A.V. Belitsky, (1997), hep-ph/9703432.

[126] M. Gluck, E. Reya and A. Vogt, Z. Phys. C67 (1995) 433.

[127] H. Avakian et al., Phys. Rev. D81 (2010) 074035, hep-ph/1001.5467.

[128] J. Balla, M.V. Polyakov and C. Weiss, Nucl. Phys. B510 (1998) 327, hep-ph/9707515.

[129] B. Dressler and M.V. Polyakov, Phys. Rev. D61 (2000) 097501, hep-ph/9912376.

[130] M. Wakamatsu, Phys. Lett. B509 (2001) 59, hep-ph/0012331.

[131] H. Avakian et al., JLab Experiment E12-07-015 (2008).

[132] L. Trentadue and G. Veneziano, Phys. Lett. B323 (1994) 201.

[133] M. Anselmino, V. Barone and A. Kotzinian, Phys. Lett. B699 (2011) 108, 1102.4214.

[134] A. Kotzinian, DIS20011 .

[135] A. Vossen et al., (2011), private communication.

[136] H. Avakian et al., JLab Experiment E12-06-015 (2008).

[137] H. Avakian et al., JLab Experiment E12-09-008 (2009).

[138] H. Avakian et al., JLab Experiment E12-09-009 (2009).

[139] Jefferson Lab Hall B, S. Kuhn et al., PAC30 Proposal (2006).

[140] J. Lachniet et al., (2008), nucl-ex/0811.1716.

[141] G. Gilfoil et al., JLab Experiment E12-07-104 (2007).

[142] R.N. Cahn, Phys. Lett. B78 (1978) 269.

[143] E.L. Berger, Z. Phys. C4 (1980) 289.

[144] A. Brandenburg, V.V. Khoze and D. Mueller, Phys. Lett. B347 (1995) 413, hep-ph/9410327.

[145] A. Afanasev, C.E. Carlson and C. Wahlquist, Phys. Lett. B398 (1997) 393, hep-ph/9701215.

[146] S.J. Brodsky et al., Phys. Lett. B449 (1999) 306, hep-ph/9812277.

[147] I. Akushevich, N. Shumeiko and A. Soroko, Eur. Phys. J. C10 (1999) 681, hep-ph/9903325.

[148] I. Akushevich, A. Ilyichev and M. Osipenko, (2007), hep-ph/0711.4789.

[149] CLAS, K.V. Dharmawardane et al., Phys. Lett. B641 (2006) 11, nucl-ex/0605028.

[150] H. Avakian and P. Bosted., (2006).

[151] L. Mankiewicz, A. Schafer and M. Veltri, Comput. Phys. Commun. 71 (1992) 305.

[152] J. Levelt and P.J. Mulders, Phys. Lett. B338 (1994) 357, hep-ph/9408257.

[153] A.M. Kotzinian et al., (1999), hep-ph/9908466.

[154] A. Metz and M. Schlegel, Eur. Phys. J. A22 (2004) 489, hep-ph/0403182.

[155] J.C. Collins and A. Metz, Phys. Rev. Lett. 93 (2004) 252001, hep-ph/0408249.